BALANCING A THREE MASS ROTOR WITH SHAFT BOW

Prepared by:

William Foiles
Graduate Student

E. J. Gunter
Professor

Rotor Dynamics Laboratory
RESEARCH LABORATORIES FOR THE ENGINEERING SCIENCES
SCHOOL OF ENGINEERING AND APPLIED SCIENCE
UNIVERSITY OF VIRGINIA
CHARLOTTESVILLE, VIRGINIA

June 1982

I. ROTOR SYSTEM

Figure 1 represents a schematic diagram of the vertical three-mass rotor-bearing system developed in the Rotor Dynamics Laboratory. The system is an adaptation of one of the Bently rotor models. The shaft diameter is 0.375 inches and the total shaft length is approximately 27 inches long. In this particular rotor, three discs of 812 grams each were mounted symmetrically on the rotor shaft. The rotor is mounted on a vertical test stand as shown in Figure 2.

Figure 3 represents a schematic diagram of the instrumentation for the vertical rotor-bearing system and the horizontal Centritech rotor which is mounted on the same horizontal concrete slab. A control panel was constructed so that the vibration signals from any of the three rotor configurations can be connected into an 8-channel FM tape recorder. The Bently Digital Vector Filters can analyze the vibration signals either directly, or after passing through the FM recorder.

Figure 4 represents a cross section of the vertical rotor-bearing system showing the setup of the horizontal and vertical probes at a typical shaft location. There are three mounting brackets with horizontal and vertical Bently displacement type probes monitoring the rotor motion at three axial planes. The location of these monitoring stations may be changed, as the holes for the mounting brackets are located on one inch centers. The horizontal and vertical probes to monitor the shaft motion are slightly offset so as not to induce cross-coupling signals due to their close proximity.

BALANCING A THREE MASS ROTOR WITH SHAFT BOW

I. ROTOR SYSTEM

Figure 1 represents a schematic diagram of the vertical three-mass rotor-bearing system developed in the Rotor Dynamics Laboratory. The system is an adaptation of one of the Bently rotor models. The shaft diameter is 0.375 inches and the total shaft length is approximately 27 inches long. In this particular rotor, three discs of 812 grams each were mounted symmetrically on the rotor shaft. The rotor is mounted on a vertical test stand as shown in Figure 2.

Figure 3 represents a schematic diagram of the instrumentation for the vertical rotor-bearing system and the horizontal Centritech rotor which is mounted on the same horizontal concrete slab. A control panel was constructed so that the vibration signals from any of the three rotor configurations can be connected into an 8-channel FM tape recorder. The Bently Digital Vector Filters can analyze the vibration signals either directly, or after passing through the FM recorder.

Figure 4 represents a cross section of the vertical rotor-bearing system showing the setup of the horizontal and vertical probes at a typical shaft location. There are three mounting brackets with horizontal and vertical Bently displacement type probes monitoring the rotor motion at three axial planes. The location of these monitoring stations may be changed, as the holes for the mounting brackets are located on one inch centers. The horizontal and vertical probes to monitor the shaft motion are slightly offset so as not to induce cross-coupling signals due to their close proximity.

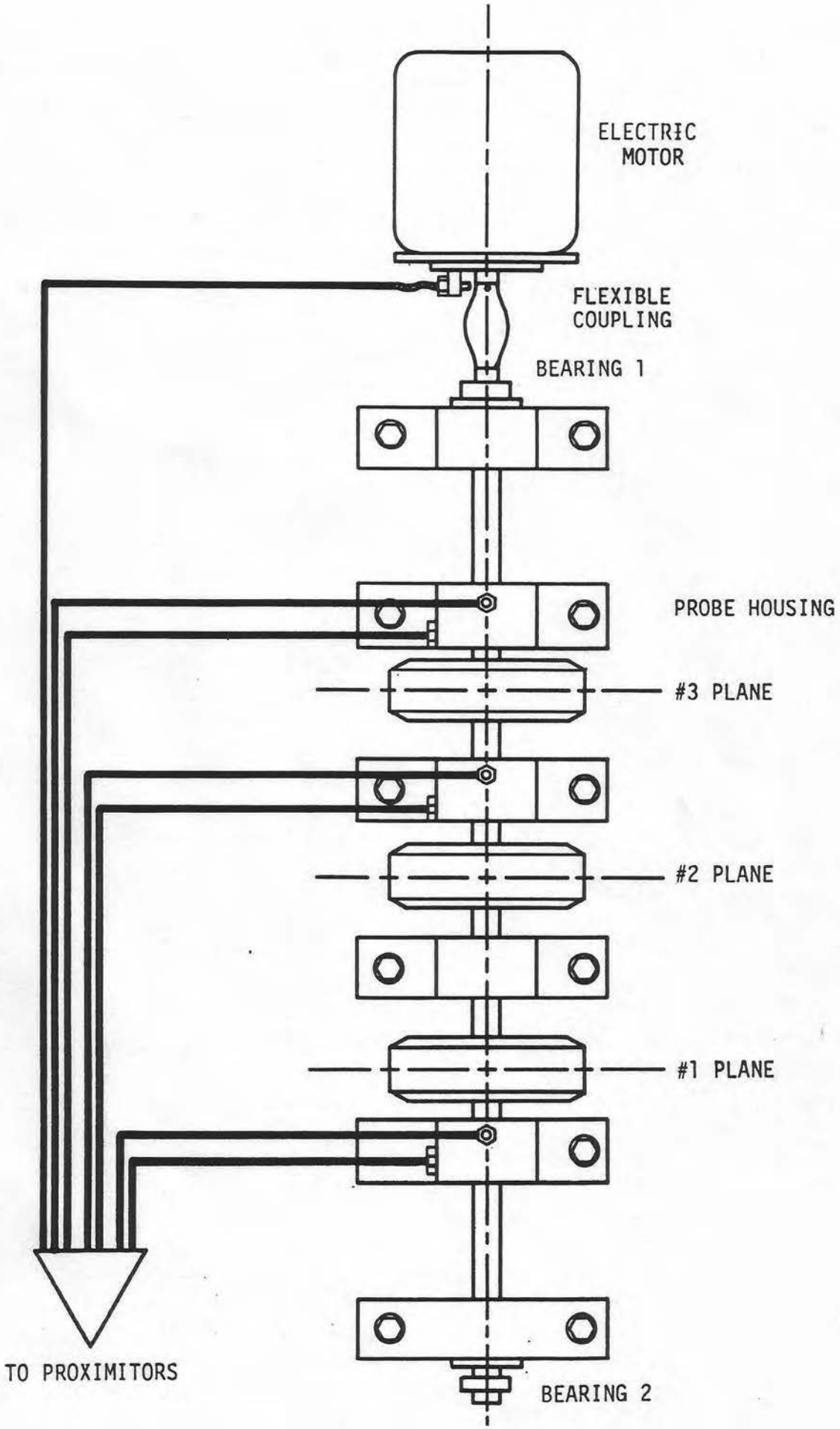

Figure 1. Schematic Diagram of Vertical Three-Mass Rotor-Bearing System (Bently Nevada Corporation)

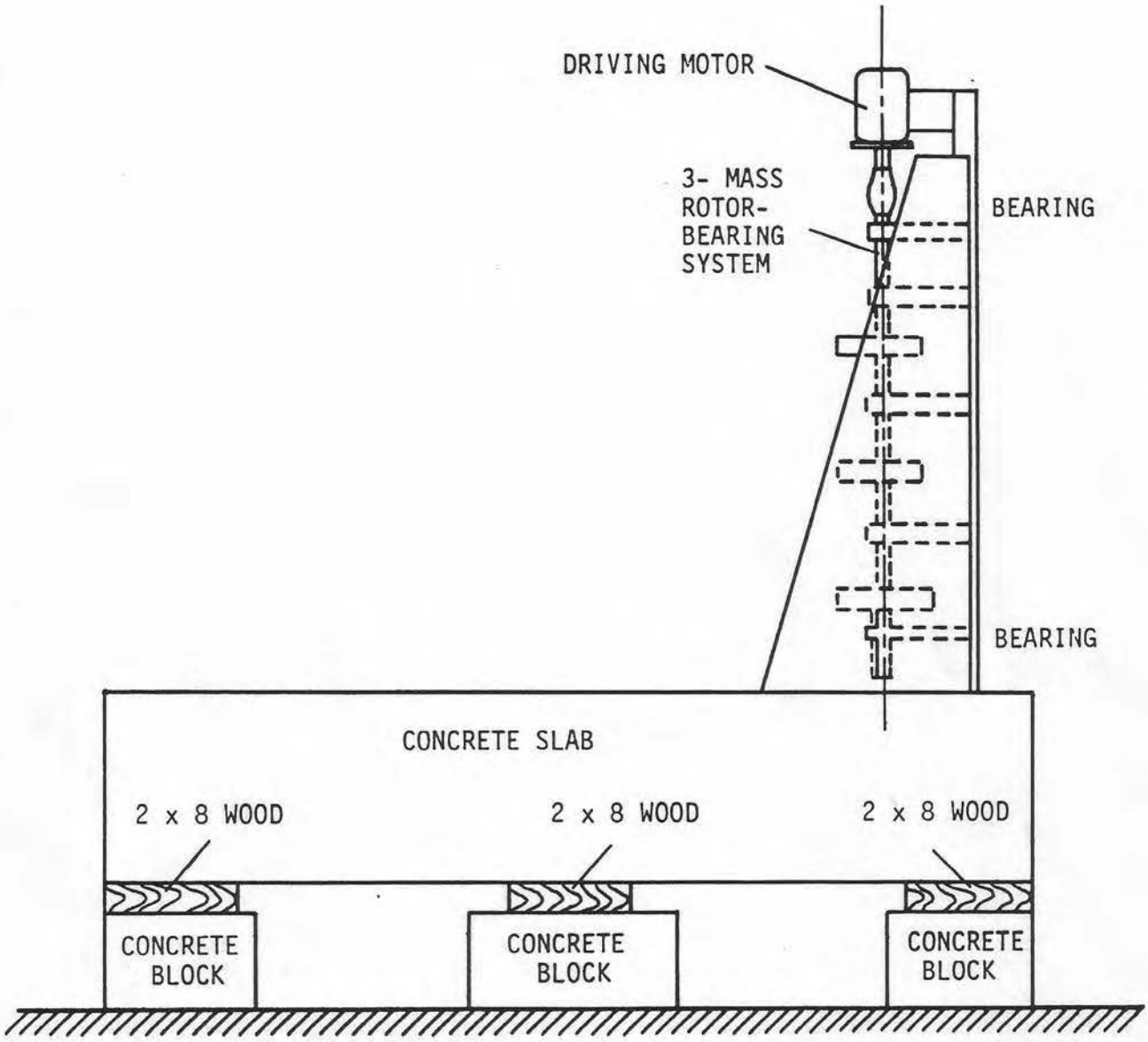

Figure 2. Schematic Diagram of Rotor-Bearing System and Foundation

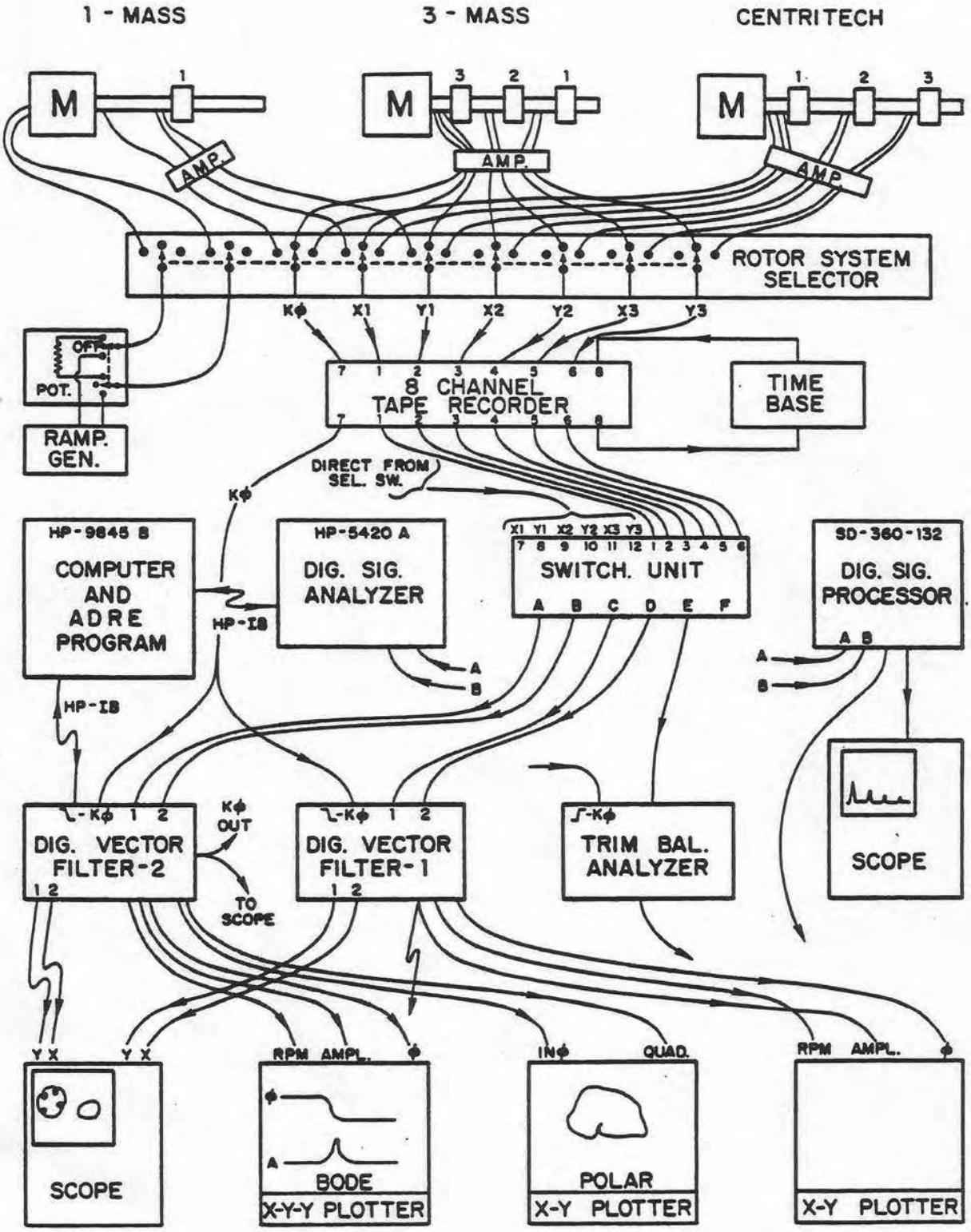

Figure 3 Block Diagram of Experimental Equipment and Instrumentation

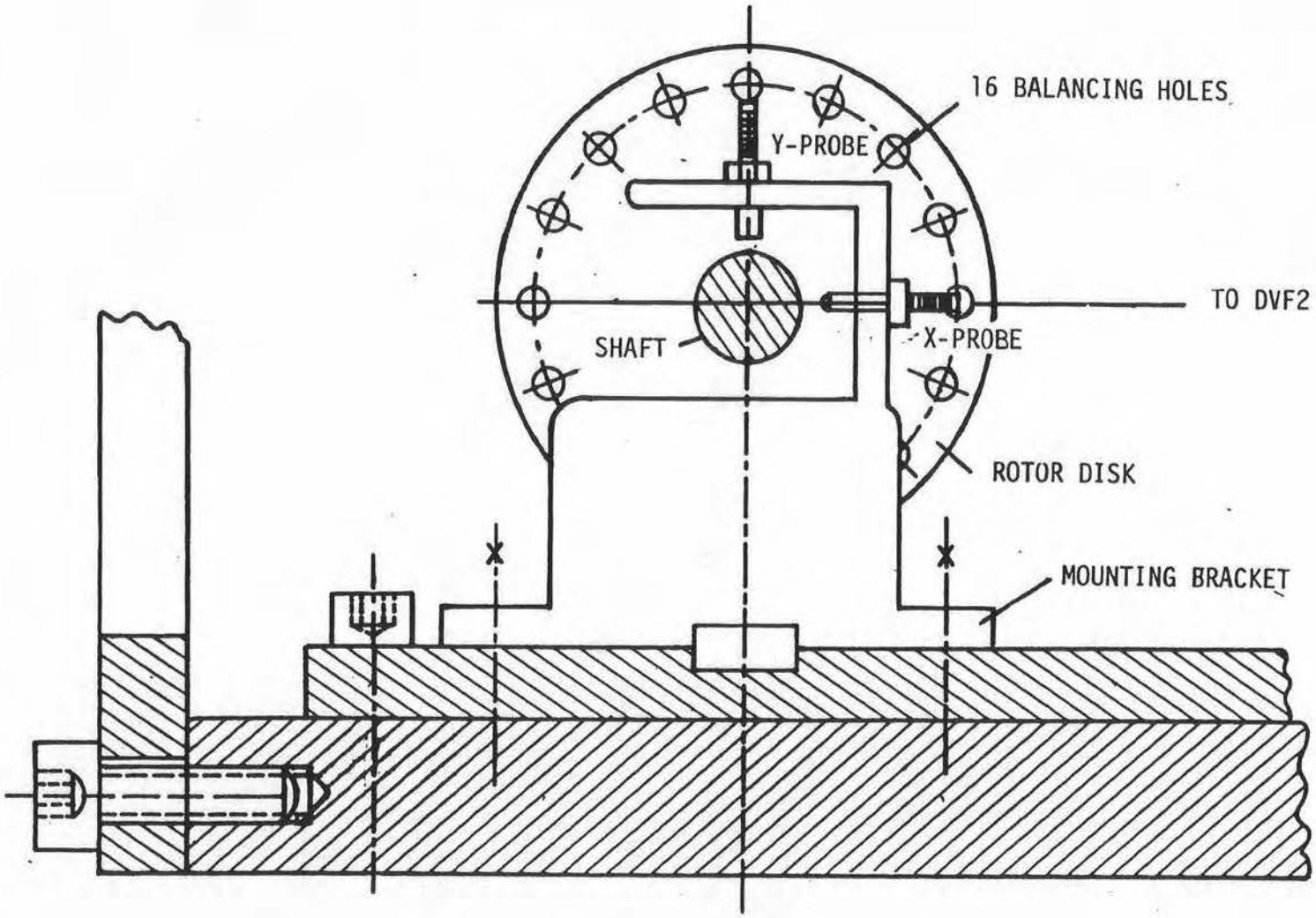

Figure 4. Rotor Cross Section Showing Typical Probe Configuration

In addition to the X-Y probes to monitor the shaft motion, an additional probe called the key phasor is mounted to sense a notch on the coupling end. The key phasor probe is essential in order to trigger the DVF. If the key phasor signal is lost, then one cannot perform the rotor synchronous amplitude and phase analysis.

Figure 5 represents a typical schematic diagram of the relationship between the key phasor and a vibration probe. When the timing notch passes under the key phasor, a pulse is generated. The phase angle as shown on the DVF represents the angle measured from the key phasor mark to the peak vibration signal of the corresponding probe being analyzed. Therefore, this angle then may be used to determine the high spot of the rotor motion. For example, if the rotor Y-motion indicates a phase angle of 45°, then one can determine the high spot of the vibrational amplitude by aligning the key phasor with the timing notch. One would then proceed to rotate 45° from the Y-probe opposite the direction of rotation. This position would determine the instantaneous high spot of the rotor vibration. Therefore, the phase angle that is observed on the DVF is a phase lag angle.

II. SYSTEM CRITICAL SPEEDS

A critical speed analysis of the vertical three mass test rig was performed with duplex bearing at the coupling end. The predicted and theoretical critical speeds were in close agreement.

Figure 6 represents an animated mode shape for the first critical speed. In this model, the discs are not assumed to be integral with

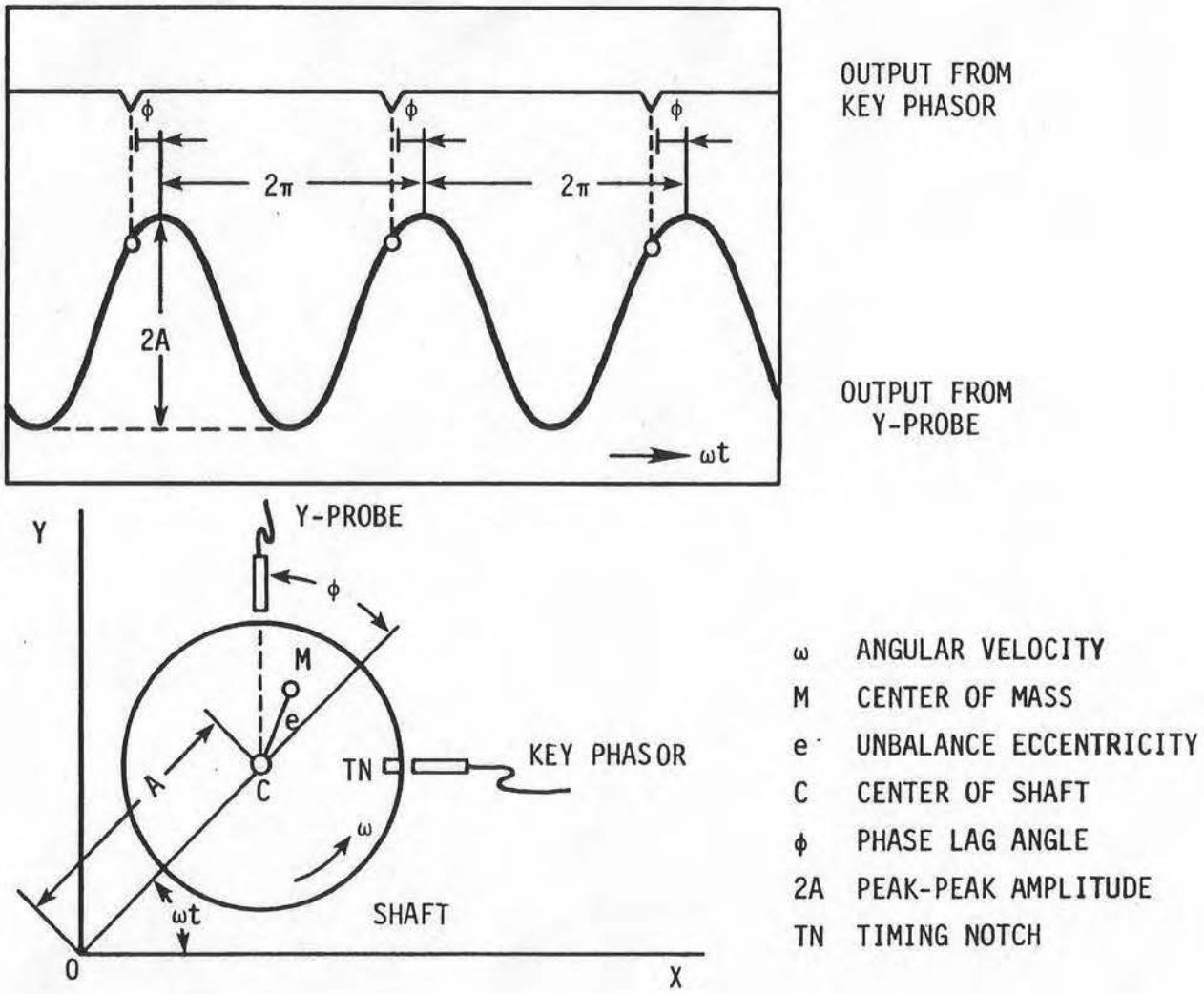

Figure 5. Relationship Between Key Phasor and Proximity Probe Output

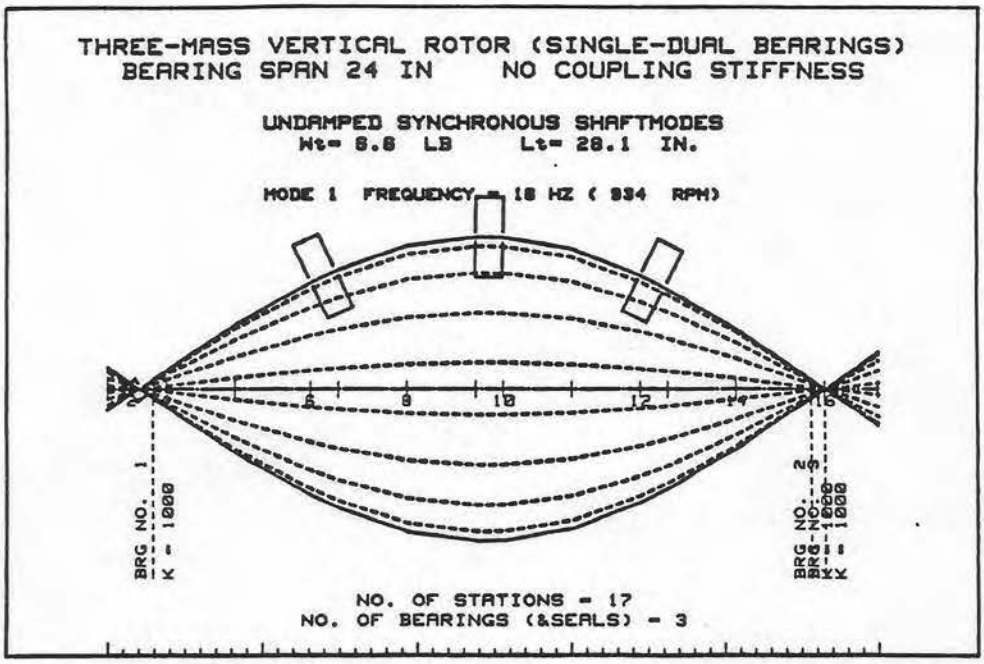

Figure 6. Animated Mode Shape Plot for the First Critical Speed (single-dual bearing system)

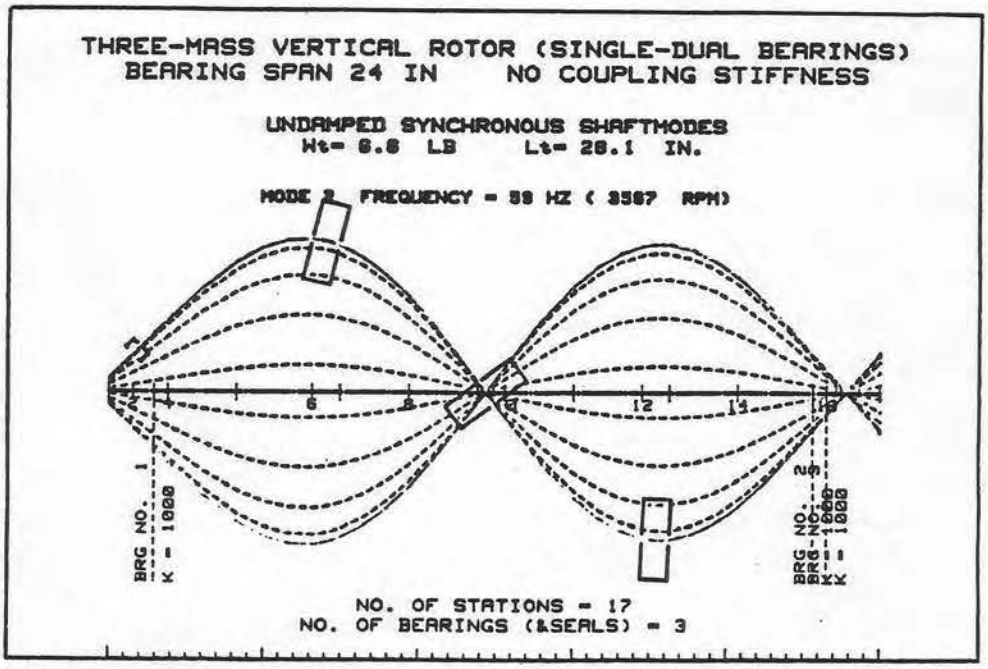

Figure 7. Animated Mode Shape Plot for the Second Critical Speed (single-dual bearing system)

the shaft. In this assumption, the discs then are drawn on the animated plot. From the observation of the mode shape, it can be seen that the third bearing is located at a nodal point.

Table 1 represents the first critical speed mode shape for the single-dual bearing system. The first critical speed is 934 RPM. Only 7% of the total strain energy is associated with the bearing deflections. The third bearing contributes no strain energy to this system and therefore does not substantially influence the rotor first critical speed. The duplex bearing was installed to control self-excited whirl instability.

Figure 7 represents the second critical speed of the single-dual bearing system and is predicted to be 3,567 RPM. Note, from the observation of the animated mode shape, that the maximum amplitude of motion occurs at the first and third discs. Notice that the amplitudes of these discs are approximately equal and the motions are out of phase. The center disc is at a nodal point. Therefore, radial unbalance weights located at station 2 will have little effect on balancing the rotor second critical speed. The rotor second critical speed can best be balanced by modal weights which are equal and placed 180° out of phase to each other at the first and third planes. Also in the experimental investigation, one should observe motion which is out of phase with respect to each other at the first and third plane locations.

Table 2 represents the modal data for the second critical speed of the single-dual bearing system. The second mode has a total strain energy of only 15% associated with the bearings.

Table 1

Table of the First Critical Speed Mode Shape of Vertical Three-Mass Rotor, Single-Dual Bearing System, 24" Bearing Span, No Coupling Stiffness

UNDAMPED ROTOR MODE SHAPES AND ENERGY DISTRIBUTION
WITH TRANSVERSE SHEAR DEFORMATION
SYNCHRONOUS FORWARD MODE SHAPES

NO. 1 CRITICAL SPEED = 934 RPM

ST	X	θ	M	V	Us	Ub	Kb	Ttr	Trot
1	-.138	.216	0.0000	0.0000				0	0
2	-.029	.216	-.0000	-.0000				0	0
3	.063	.216	-.0000	-.0000	0	4	1,000	0	0
4	.125	.216	-.0020	-.0033				0	0
5	.423	.199	-.0120	-.0033	1			0	0
6	.703	.154	-.0229	-.0032	7			12	-0
7	.788	.142	-.0256	-.0023	2			16	0
8	.944	.076	-.0296	-.0013	15			2	0
9	1.000	.002	-.0332	-.0012	20			23	-0
10	.996	-.015	-.0331	.0001	5			23	0
11	.921	-.089	-.0289	.0014	19			2	0
12	.748	-.152	-.0244	.0015	14			13	-0
13	.659	-.163	-.0214	.0024	2			10	0
14	.395	-.202	-.0113	.0033	6			0	0
15	.063	-.217	-.0001	.0033	1	4	1,000	0	0
16	.001	-.217	-.0000	.0001	0	0	1,000	0	0
17	-.240	-.217	-.0000	.0000				0	0
					93	7		100	-0

Utotal = 53.12; Ttotal = 53.14; ERROR ENERGY BALANCE = -.0%

Modal Weight W_1 = 4.3 LB

Table 2

Table of the Second Critical Speed Mode Shape of Vertical Three-Mass Rotor, Single-Dual Bearing System, 24" Bearing Span, No Coupling Stiffness

UNDAMPED ROTOR MODE SHAPES AND ENERGY DISTRIBUTION
WITH TRANSVERSE SHEAR DEFORMATION
SYNCHRONOUS FORWARD MODE SHAPES

NO. 2 CRITICAL SPEED = 3567 RPM

ST	X	θ	M	V	Us	Ub	Kb	Ttr	Trot
1	.088	.309	0.0000	0.0000				0	0
2	.243	.309	.0000	.0000	0			0	0
3	.375	.309	.0002	.0002	0	10	1,000	0	0
4	.463	.307	-.0115	-.0191	0			0	0
5	.849	.211	-.0688	-.0187	3			1	0
6	1.000	-.045	-.1276	-.0174	16			25	-0
7	.956	-.109	-.1259	.0015	5			23	0
8	.621	-.336	-.0660	.0196	14			1	0
9	.065	-.418	-.0032	.0205	2			0	-1
10	-.173	-.414	.0212	.0217	0			1	0
11	-.696	-.297	.0778	.0185	4			1	0
12	-.957	-.048	.1313	.0174	16			23	-0
13	-.966	.017	.1303	-.0006	5			23	0
14	-.753	.258	.0726	-.0189	16			1	0
15	-.246	.359	.0051	-.0200	3	4	1,000	0	0
16	-.143	.360	.0004	-.0075	0	1	1,000	0	0
17	.257	.361	.0000	-.0001				0	0
					85	15		100	-0

Utotal = 722.4; Ttotal = 723.7; ERROR ENERGY BALANCE = -.2%

Modal Weight W_2 = 4.0 LB

Figure 8 represents the animated mode shape for the third mode of the single-dual bearing system. It is of interest to note that the first and third discs are now in phase at the third mode and the center disc is out of phase to the first and third discs. Modal correction weights for the third mode, therefore, will require three planes of balancing with the center balancing correction out of phase to the end components. The critical speed mode shape data will be used to generate these modal components, see Table 3.

Table 4 represents the critical speed summary for the single-dual bearing system. The corresponding mode shape summary is shown in Figure 9. In comparison of the critical speed summary for the single bearing system (Table 5) with the dual bearing system (Table 4) it can be seen that there is no substantial difference in the critical speeds. In the second model, there is, in general, a slight reduction in the rotor modal masses of the first and second critical speeds.

III. ROTOR ANALYTIC MODEL

A computer model was developed to simulate the three-mass vertical test rotor. In the critical speed analysis, 17 stations were used to simulate the rotor model. The actual rotor has a duplex bearing at the top which causes the rotor model to be slightly asymmetric. In the simplified mathematical model developed for the three-mass vertical test rig, a five station model was generated. The stiffness matrix corresponds to the stiffness matrix contained with the 24-inch shaft mounted on symmetric springs of 1,000 lb/in at each end. Masses of .00465 lb-sec^2/in [1.795 lb] were used to simulate the mass at each disc. The system general equations of motion are as follows:

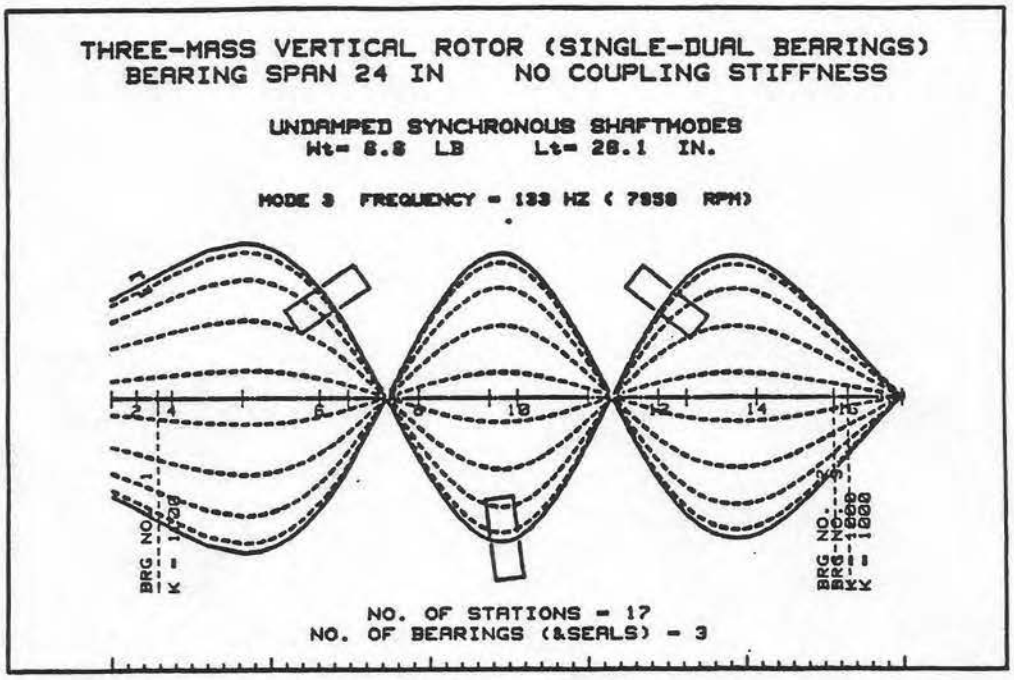

Figure 8. Animated Mode Shape Plot for the Third Critical Speed (single-dual bearing system)

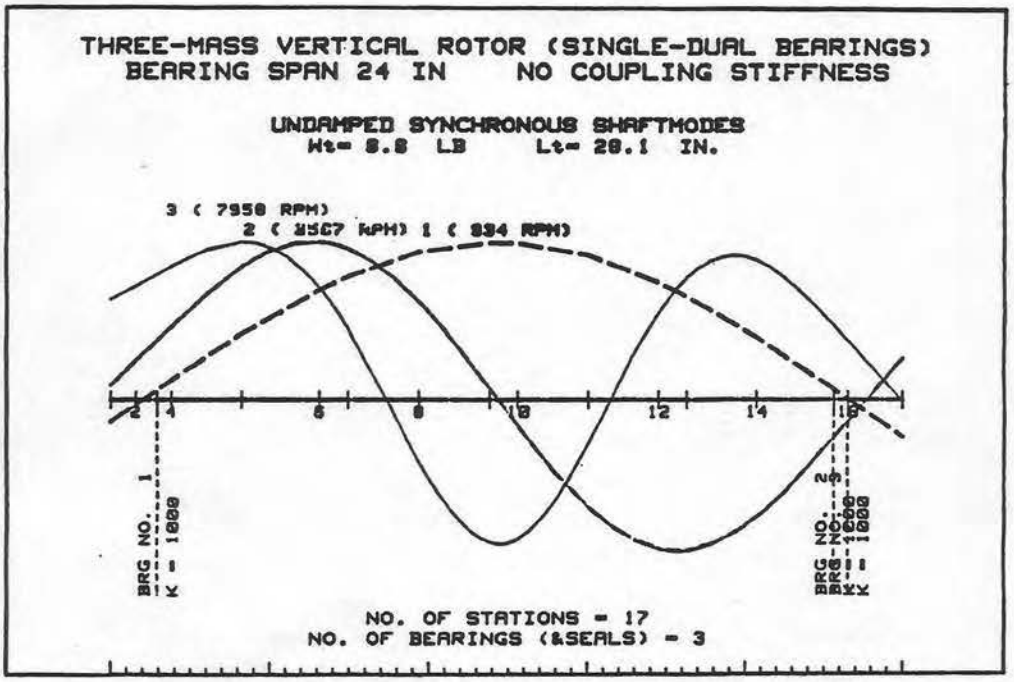

Figure 9. Mode Shapes of the First Three Critical Speeds (single-dual bearing system)

Table 3

Table of the Third Critical Speed Mode Shape of Vertical Three-Mass Rotor, Single-Dual Bearing System, 24" Bearing Span, No Coupling Stiffness

UNDAMPED ROTOR MODE SHAPES AND ENERGY DISTRIBUTION
WITH TRANSVERSE SHEAR DEFORMATION
SYNCHRONOUS FORWARD MODE SHAPES

NO. 3 CRITICAL SPEED = 7958 RPM

ST	X	θ	M	V	Us	Ub	Kb	Ttr	Trot
1	.637	.171	0.0000	0.0000				0	0
2	.723	.171	.0008	.0008				1	0
3	.796	.172	.0039	.0034	0	10	1,000	0	0
4	.845	.169	-.0183	-.0363				1	0
5	1.000	.007	-.1183	-.0326	2			2	0
6	.713	-.412	-.2023	-.0250	10			15	-1
7	.450	-.505	-.1611	.0423	3			6	0
8	-.399	-.579	.0981	.0845	2			0	0
9	-.919	-.047	.3492	.0816	19			24	-0
10	-.896	.126	.3421	-.0048	9			23	0
11	-.289	.614	.0698	-.0890	16			0	0
12	.549	.446	-.2104	-.0911	4			9	-1
13	.772	.334	-.2472	-.0395	4			17	0
14	.885	-.134	-.1465	.0331	13			2	0
15	.466	-.340	-.0120	.0399	3	3	1,000	0	0
16	.369	-.343	-.0005	.0179	0	2	1,000	0	0
17	-.012	-.343	-.0002	.0000				0	0
					84	16		101	-1

Utotal = 3,133; Ttotal = 3,147; ERROR ENERGY BALANCE = -.5%

Modal Weight W_3 = 3.5 LB

Table 4

Critical Speed Summary of Vertical Three-Mass Rotor, Single-Dual Bearing System, 24" Bearing Span, No Coupling Stiffness

SYNCHRONOUS CRITICAL SPEED ANALYSIS WITH TRANSVERSE SHEAR DEFORMATION

Brg. NO. 1 ST. 3 Kb = 1000 Lb/In
Brg. NO. 2 ST. 15 Kb = 1000 Lb/In
Brg. NO. 3 ST. 16 Kb = 1000 Lb/In

NO.	CRITICAL SPEED (RPM)	(HZ)	Wmode (LB)	Imode= It-(v/ω)Ip (LB)	WTmode (LB)	Kmode (LB/IN)	Us (-)	Ub (-)	Ttr (-)	Trot (-)
1	934	(16)	4.29	-.00	4.3	106	93	7	100	-0
2	3,567	(59)	4.02	-.02	4.0	1,447	85	15	100	-0
3	7,958	(133)	3.53	-.03	3.5	6,295	84	16	101	-1

Table 5

Critical Speed Summary of Vertical Three-Mass Rotor,
24" Single Bearing Span. No Coupling Stiffness

SYNCHRONOUS CRITICAL SPEED ANALYSIS WITH TRANSVERSE SHEAR DEFORMATION

Brg. NO. 1 ST. 2 Kb = 1000 Lb/In
Brg. NO. 2 ST. 13 Kb = 1000 Lb/In

NO.	CRITICAL SPEED (RPM)	(HZ)	Wmode (LB)	Imode = It-(v/ω)Ip (LB)	WTmode (LB)	Kmode (LB/IN)	Us (-)	Ub (-)	Ttr (-)	Trot (-)
1	937	(16)	4.45	-.00	4.4	111	92	8	100	-0
2	3,528	(59)	4.27	-.02	4.3	1,504	79	21	100	-0
3	7,897	(132)	3.47	-.05	3.4	6,065	78	22	101	-1

$$
\begin{bmatrix} [M] & & & \\ & [I_t] & & \\ & & [M] & \\ & & & [I_t] \end{bmatrix}_m \begin{Bmatrix} \{\ddot{x}\} \\ \{\ddot{\theta}_x\} \\ \{\ddot{y}\} \\ \{\ddot{\theta}_y\} \end{Bmatrix} + \begin{bmatrix} & & \omega[I_p] & \\ & & & \\ & -\omega[I_p] & & \\ & & & \end{bmatrix}_G \begin{Bmatrix} \{\dot{x}\} \\ \{\dot{\theta}_x\} \\ \{\dot{y}\} \\ \{\dot{\theta}_y\} \end{Bmatrix}
$$

$$
\begin{bmatrix} [C_{xx}] & & [C_{xy}] & \\ & [C_{\theta\theta}] & & \\ [C_{yx}] & & [C_{yy}] & \\ & & & [C_{\phi\phi}] \end{bmatrix}_c \begin{Bmatrix} \{\dot{x}\} \\ \{\dot{\theta}_x\} \\ \{\dot{y}\} \\ \{\dot{\theta}_y\} \end{Bmatrix} +
$$

$$
\begin{bmatrix} & & K_{shaft} & \\ & & & \\ \text{sym} & & & \\ & & & \end{bmatrix}_s \begin{Bmatrix} \{x\} \\ \{\theta_x\} \\ \{y\} \\ \{\theta_y\} \end{Bmatrix} +
$$

$$
\begin{bmatrix} [K_{xx}] & & [K_{xy}] & \\ & [K_{\theta\theta}] & & \\ [K_{yx}] & & [K_{yy}] & \\ & & & [K_{\phi\phi}] \end{bmatrix}_b \begin{Bmatrix} \{x\} \\ \{\theta_x\} \\ \{y\} \\ \{\theta_y\} \end{Bmatrix} = \begin{Bmatrix} \{P_x\ (t)\} \\ \{M_x\ (t)\} \\ \{P_y\ (t)\} \\ \{M_y\ (t)\} \end{Bmatrix} \qquad (3.1)
$$

From the standpoint of unbalance response and balancing calculations the five stations model is adequate to represent the rotor dynamical characteristics. Since the rotor gyroscopic effects are minimal for the three modes in the operating speed range, the rotor X and Y equations of motion for synchronous response may be considered to be uncoupled. The rotor equations of motion for the X direction for example reduces to the following.

$$M \begin{bmatrix} 0.0 & & & & \\ & 1.0 & & & \\ & & 1.0 & & \\ & & & 1.0 & \\ & & & & 0.0 \end{bmatrix} \begin{Bmatrix} \ddot{X}_1 \\ \ddot{X}_2 \\ \ddot{X}_3 \\ \ddot{X}_4 \\ \ddot{X}_5 \end{Bmatrix} +$$

$$C \begin{bmatrix} 1.0 & & & & \\ & 0.4 & & & \\ & & 0.4 & & \\ & & & 0.4 & \\ & & & & 1.0 \end{bmatrix} \begin{Bmatrix} \dot{X}_1 \\ \dot{X}_2 \\ \dot{X}_3 \\ \dot{X}_4 \\ \dot{X}_5 \end{Bmatrix} +$$

$$K \begin{bmatrix} 1.215 & -.489 & .348 & -.089 & .015 \\ & 1.326 & -1.274 & .526 & -.089 \\ & & 1.852 & -1.274 & .348 \\ & & & 1.326 & -.489 \\ (\text{sym}) & & & & 1.215 \end{bmatrix} \begin{Bmatrix} X_1 \\ X_2 \\ X_3 \\ X_4 \\ X_5 \end{Bmatrix} =$$

$$[K] \{X\}_{bow} + \omega^2 [\{U \cos(wt + \phi)\}] \qquad (3.2)$$

Where $M = 0.00465$ Lb-sec^2/in

$C = 0.42$ Lb-sec/in

$K = 1{,}000$ Lb/in

In this model the masses are lumped only at the three major mass locations. The effective damping at the various stations was determined by a complex eigenvalue analysis used to match the theoretical damped roots with the actual system amplification factors as determined by Gunter, Springer, and Humphris in Ref (1). The matrix solution of these equations for synchronous response is given in Appendix A.

Table 6 represents the undamped normal modes and modal masses for the 5 station model. Part Two of Table 6 represents the constrained normal modes which are obtained by setting the bearing stiffness to infinity. Mathematically, this is identical to truncating the matrix by eliminating the rows and columns at which the bearing displacement occurs. As a first step in evaluating various techniques of balancing, using the least squared error approximation, the three-mass rotor unbalance response characteristics were simulated assuming a conical shaft displacement of one mil radial at the coupling end.

In the figures that follow solid lines represent rotor motion as simulated by the "Rotor" Program. Dashed lines represent runout compensated data; which is the rotor motion minus the bow vector.

Figures 10 through 14 represent the rotor motion along the various stations of the rotor for the speed range of 0 to 10,000 RPM with a conical shaft bow of 1 mil at the coupling and no unbalance. From the examination of the various figures, it is apparent that the conical shaft bow excites all of the rotor modes of system, even though individual disks do not have unbalance as such. For example, Figure 10 represents the motion at the coupling end with the one mil radial offset. At low speeds, the rotor amplitude is 2 mils peak-to-peak. It is seen that the rotor first, second and third critical speeds are excited. The largest excitation at the coupling end is observed at the second critical speed. In addition to showing the amplitude, the compensated and uncompensated phase angles are also displayed. The compensated amplitude and phase angles are obtained by subtracting the zero speed initial bow vector from the corresponding amplitudes at speed.

Table 6

Three-Mass System Mode Shapes and Eigenvalues

I		Normal Modes		
FREQ	RPM (HZ) RAD/SEC	968.6 (16.1) 101.42	3618 (60.3) 378.85	7911 (131.9) 828.4
M Modal LB-SEC^2/IN		.0095	.0093	.0091
Station	1	.057	0.334	-0.608
	2	0.724	1.000	-.6906
	3	1.000	0.0	1.00
	4	0.724	-1.000	-0.6906
	5	0.057	-0.334	-0.608

II		Constrained Normal Mode		
FREQ	RPM (HZ) RAD/SEC	995 (16.6) 104.17	3947 (66) 413.3	8470 (1412) 886.9
M Modal		.0093	.0093	.0093
Station	2	0.7071	1.00	-0.7071
	3	1.000	0.00	1.000
	4	0.7071	1.00	-0.7071

III		Free-Free Modes		
FREQ	RPM (HZ) RAD/SEC	0	0	4870.5 (81.2) 510
M Modal		.01395	0.0093	.0069
Station	1	1	2	-3.00
	2	1	1	-0.50
	3	1	0	1.00
	4	1	-1	-0.50
	5	1	-2	3.00

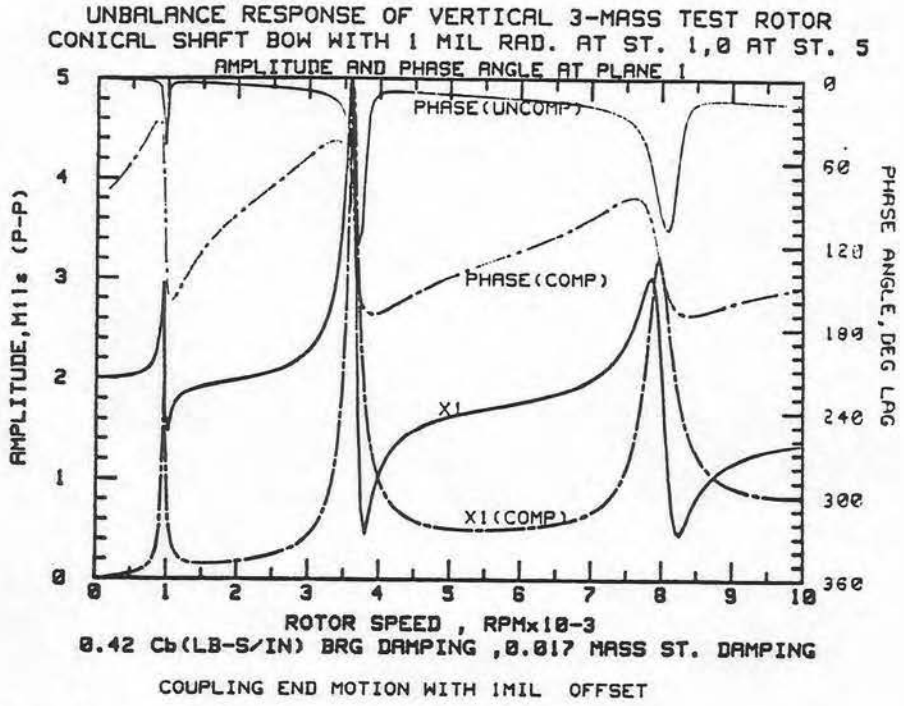

Figure 10. Compensated and Uncompensated Coupling Rotor Amplitude with One Mil Radial Conical Shaft Initial Misalignment

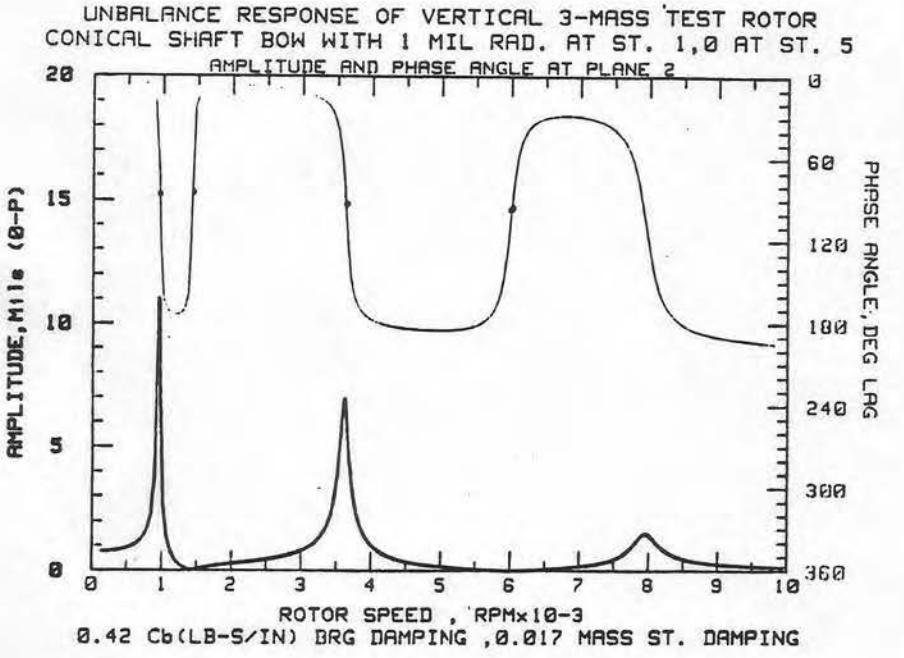

Figure 11a. First Disc (Plane 2) Rotor Amplitude and Phase with One Mil Radial Shaft Bow

In a rotor with conventional radial unbalance, a 0° to 180° phase angle shift only is observed for each rotor mode of motion. For example, at the coupling end, the phase angle shifts are observed as abrupt spikes occurring near the critical speeds. Figure 11A represents the uncompensated amplitude and phase for plane 2. After the rotor passes through the first critical speed, there is an amplitude of minimum vibration. Associated with this point of minimum vibration is a 180° phase shift. This speed may be considered as an anti-resonance speed. This phenomena will not occur with a rotor with purely mechanical unbalance. At high speed above the second critical at approximately 6,000 RPM, a second anti-resonance speed is obtained at the second plane inboard from the coupling. Figure 11B represents the plane 2, showing compensated as well as uncompensated amplitude and phase. Conventional influence coefficient balancing is normally accomplished using compensated amplitude and phase data.

Figure 12 represents the rotor motion in plane 3 which is the center span. The conical shaft bow excites the first critical speed at 958 RPM and the third critical speed at 7,945 RPM. It does not excite the second critical speed at the center plane. This is because at the center plane the second mode is a node point at this position.

Table 7 represents the maximum amplitudes of motion observed at the 5 stations over the speed range of 0 to 10,000 RPM. The maximum amplitude of motion for stations 2, 3 and 4 correspond to the first critical speed of 958 RPM. The maximum amplitude of motion is at the center span and is 30.38 mils peak-to-peak. For this particular mode, it was determined that the rotor first critical speed has an amplification

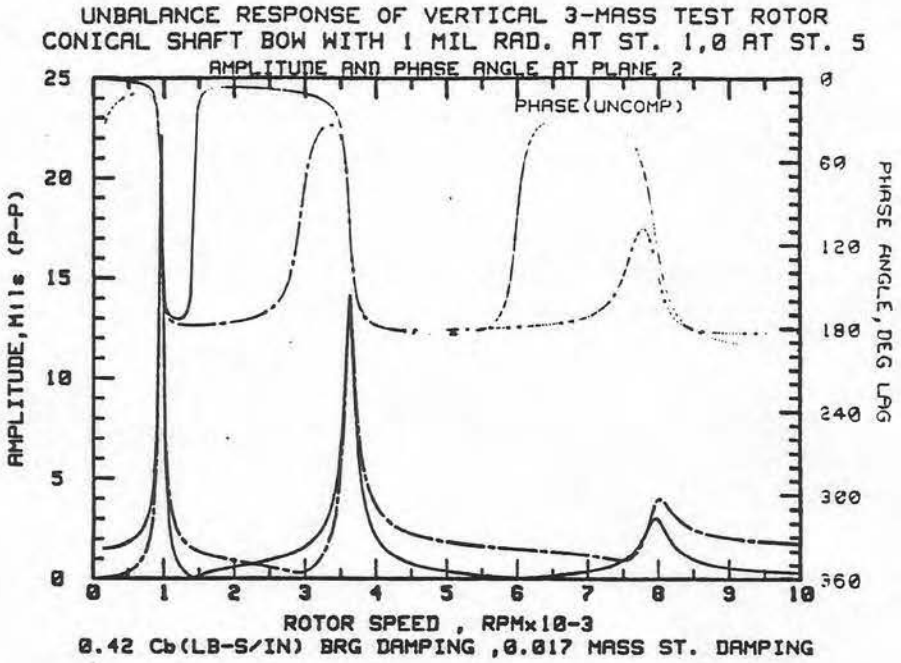

Figure 11b. Compensated and Uncompensated Rotor Amplitude and Phase at Plane 2

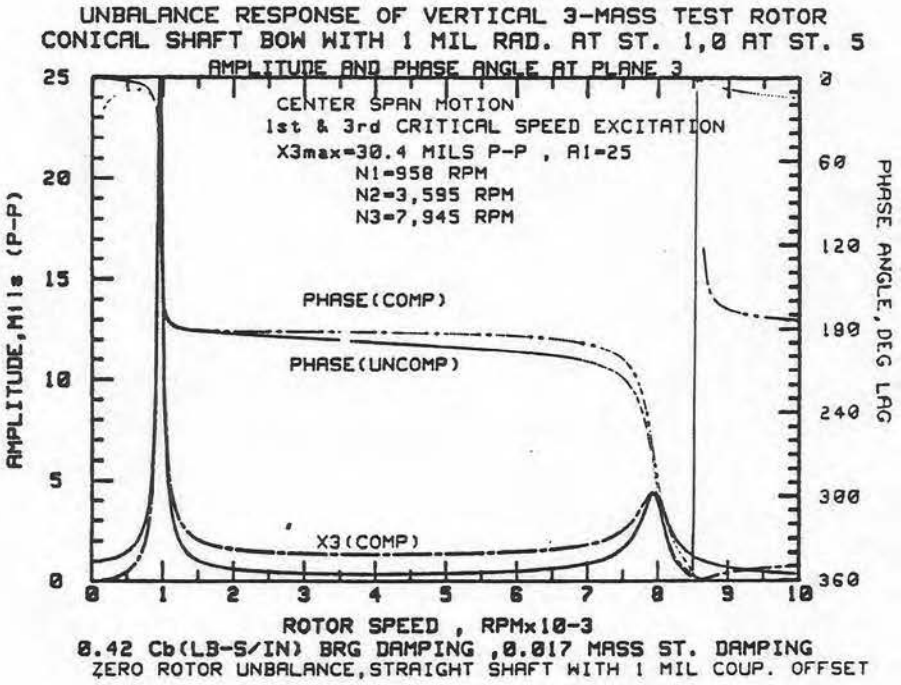

Figure 12. Compensated and Uncompensated Rotor Amplitude and Phase at Plane 3

Table 7

Unbalance Response of Vertical Three-Mass Test Rotor
Conical Shaft Bow with 1 Mil Rad. at Station 1,0 at Station 5
0.42 Cb(LB-S/IN) Brg. Damping, 0.017 Mass St. Damping

ROTOR MAXIMUM AMPLITUDES OF MOTION-
UNCOMPENSATED AND COMPENSATED

St. No.	x (MILS) (P-P)	Phase Deg Lag	Nrpm	Xc (MILS) (P-P)	Phasec Deg Lag	Nrpm	Ac (Dim)
1	5.04	62.5	3,595	4.89	109.6	3,625	26.2
2	22.03	88.7	958	22.08	95.7	959	25.3
3	30.38	90.8	958	30.45	95.7	959	25.4
4	21.99	94.6	959	22.04	95.9	959	25.4
5	4.58	289.3	3,625	4.58	289.3	3,625	28.0

factor of approximately 25.4. This amplification factor was determined by the derivative of the phase angle at the critical speed and is given as follows:

$$A_c = \frac{N_c \pi}{360} \left(\frac{d\phi^\circ}{dN}\right)\Big|_{N = N_c} \qquad (3.3)$$

It is of interest to note that for the first mode, the maximum amplitude of motion occurs at an uncompensated phase shift angle of 90.8° and at a compensated phase angle of 95.7°. For systems of higher damping, it will be observed that the maximum amplitude of motion does not occur at the undamped critical speed, but at a slightly higher speed and phase angle shift.

Table 7 also shows that the maximum amplitudes of motion at the bearings correspond to the second critical speed at 3,595 RPM at the coupling bearing and at approximately 3,625 RPM at the lower bearing. Therefore, the speeds at which the peak amplitudes occur are not necessarily the same. By a similar procedure, the amplification factor for the second critical speed was determined to be approximately 26-28.

Figure 13 represents the uncompensated rotor phase and amplitude of motion of plane 4 (disc 3). The phase angles show a conventional 0° to 180° shift for each mode. Figure 14 represents the amplitude and phase for the lower bearing, station number 5.

In the unbalance response curves shown, it is seen that the rotor will be excited at all three modes simply by physically displacing the coupling alignment by 1 mil even though the rotor is mechanically perfectly balanced by itself. It appears to exhibit all of the characteristics of a typically unbalanced rotor. The presence of shaft

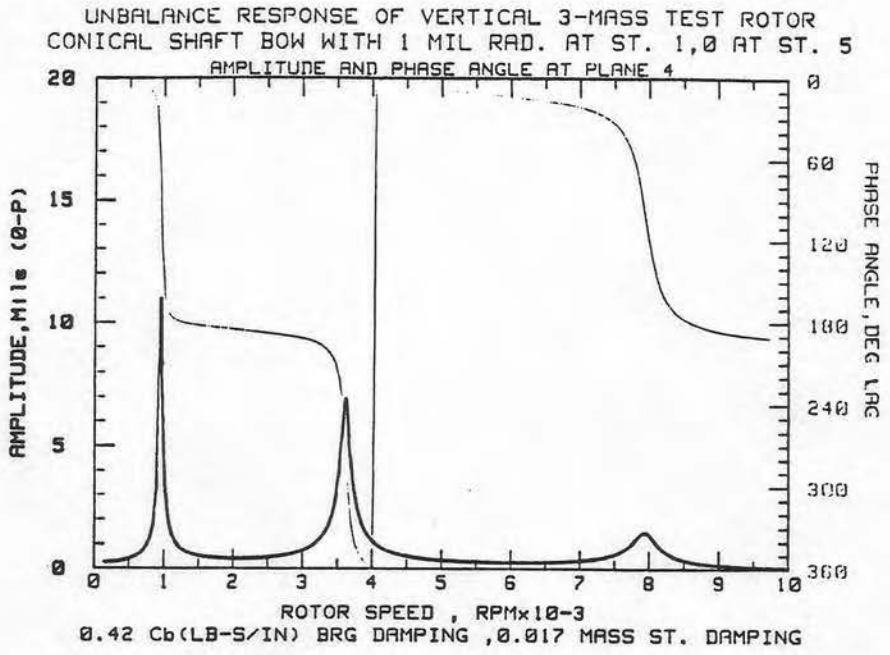

Figure 13. Uncompensated Rotor Amplitude and Phase at Plane 4

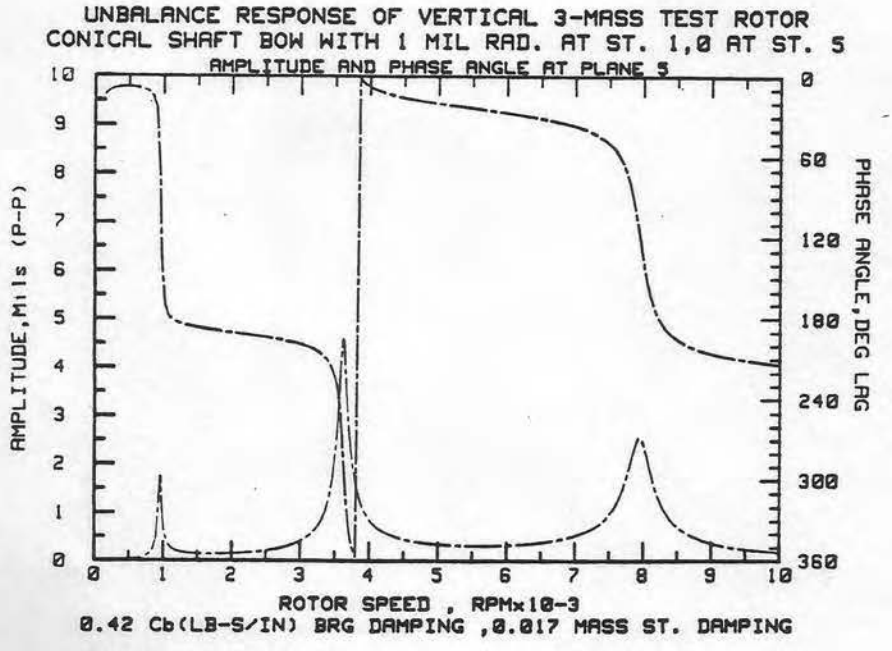

Figure 14. Compensated Rotor Amplitude and Phase at Plane 5

misalignment, however, causes the occurrence of resonance and anti-resonance speeds which is not seen in the case of conventional unbalance alone.

IV. ROTOR BALANCING

The rotor will be balanced in two ways, both techniques will employ the computer program "LINLS." First, trial weights will be added to each of the balance planes (planes 2, 3 and 4) one at a time. The readings will be recorded and "LINLS" will be used to predict the corrective balances.

Second, modal trial weights will be added. In this case a trial weight will consist of a set of trial weights distributed among the planes. The distribution will be $M\phi_i$, where M is the mass matrix and ϕ_i is a multiple of the i^{th} mode shape. These readings will be recorded and "LINLS" will predict the final balance.

4.1 Balancing Using Conventional Trial Weights

Using the program ROTOR, a trial weight of 0.5 gm-in has been added in turn to each of the three discs at 180°. The trial weight was first added to disc 1; the results are shown in Figs. 15 and 16. Figure 15 shows the effect of the trial weight at plane 2 is to lower the responses at the first and second critical speeds. The response of the third critical speed increased slightly. Figure 16 shows similar results for plane 3. Note again that this station is a node point for the second critical speed.

In the graphs produced by the ROTOR program solid lines for amplitude and phase angle represent the actual rotor motion.

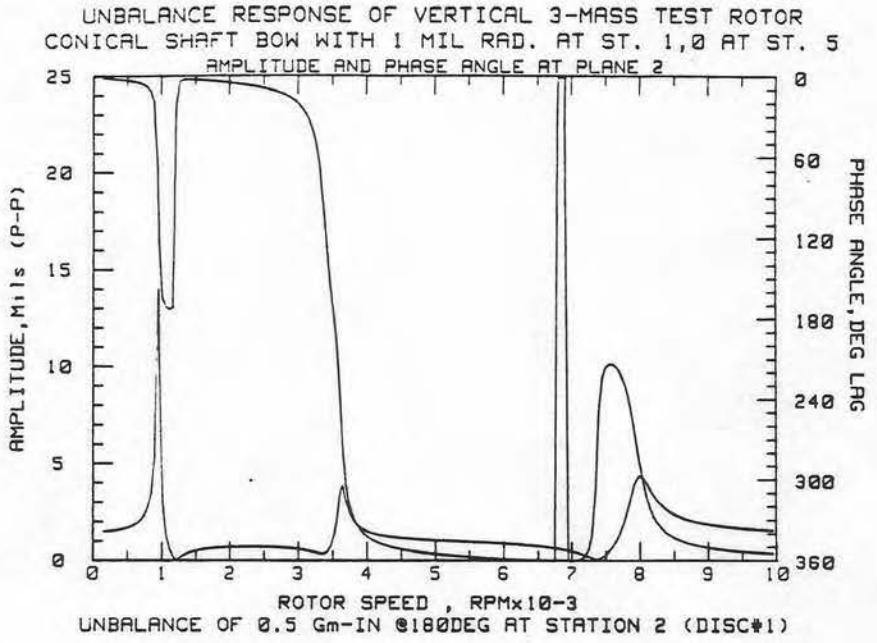

Figure 15. Unbalance Response at Station 2 with 0.5 gm-in with Trial Unbalance of 180 Degrees at Station 2

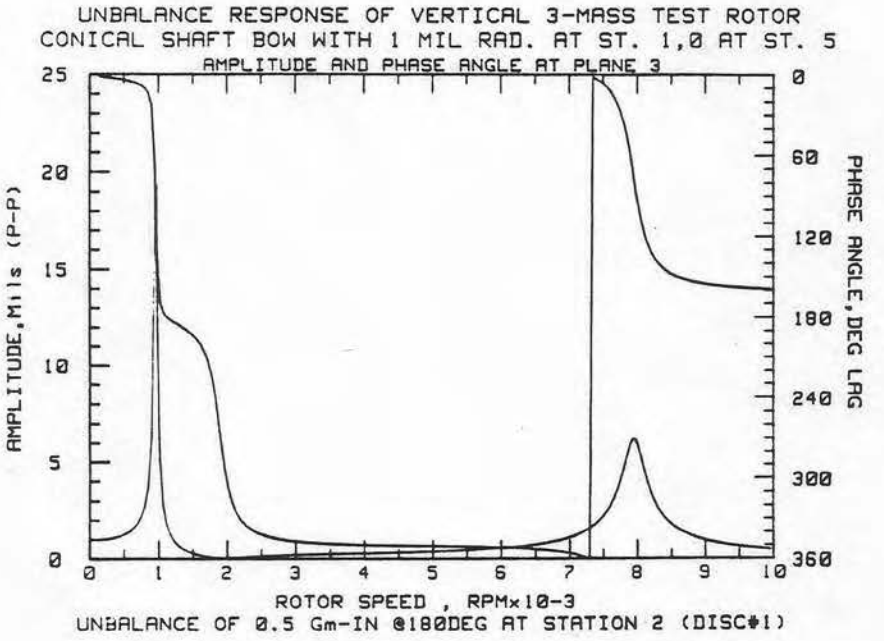

Figure 16. Unbalance Response at Station 3 with Trial Unbalance of 0.5 gm-in at 180 Degrees at Station 3

Dashed lines for amplitude and phase angle are the compensated readings; actual shaft motion minus shaft bow.

Next the trial weight is removed from disc 1 (balance plane 1) and a trial weight of 0.5 gm-in at 180° is added to disc 2. It is important to note that the previous trial weight was removed. The results of this are shown in Figures 17 and 18.

Finally, the trial weight at disc 2 (balance plane 2) are removed, and a trial weight of .5 gm-in at 180° is added to disc 3 (balance plane 3). The results are shown in Figures 19 and 20.

The important points of this example so far are:

1. The initial measurements are recorded.
2. A trial weight is added to balance plane 1 with the other balance planes left in their original state. The results are recorded.
3. The previous trial weight is removed from balance plane 1 and a trial weight is added to balance plane 2. The results are recorded.
4. The previous trial weight is removed from balance plane 2, and a trial weight is added to balance plane 3. The results are recorded.

In the practice of multi-plane balancing of large turbogenerators in spin pit facilities, it is often desirable to use modal or distributed trial weights along various stations, rather than the use of individual plane excitation. This procedure will be discussed in detail in the next section.

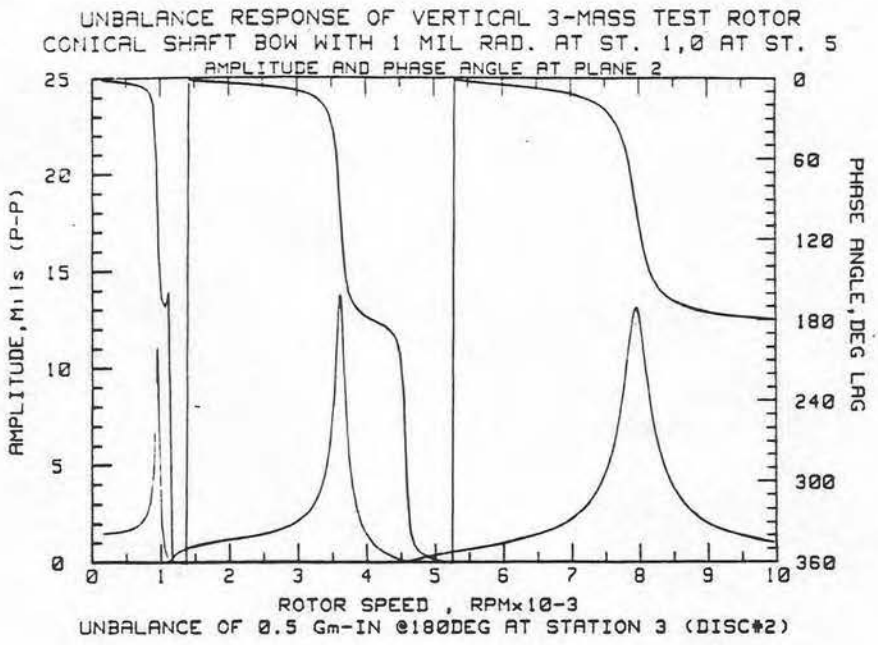

Figure 17. Unbalance Response at Station 2 with Trial Unbalance of 0.5 gm-in at 180 Degrees at Station 3

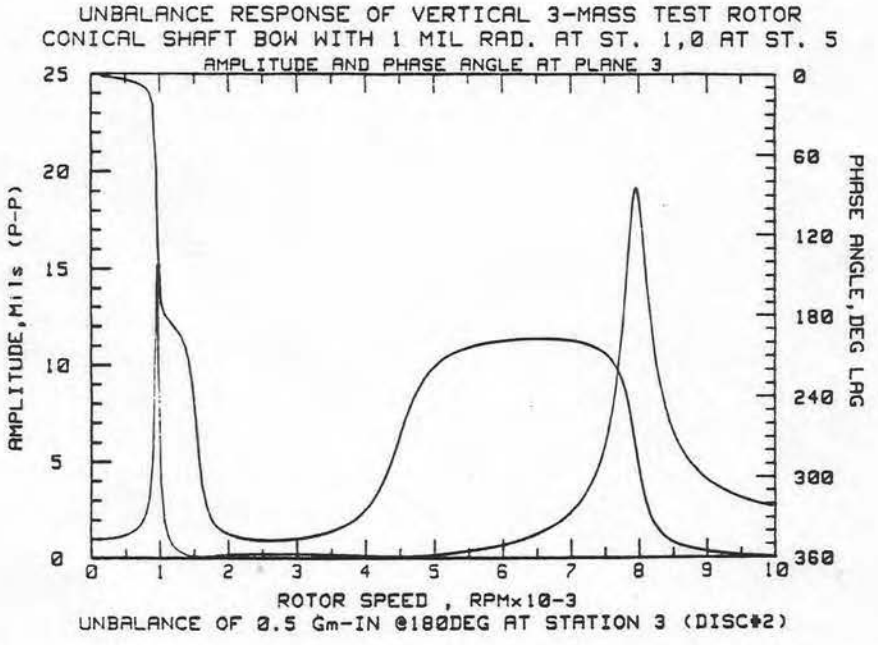

Figure 18. Unbalance Response at Station 3 with Trial Unbalance of 0.5 gm-in at 180 Degrees at Station 3

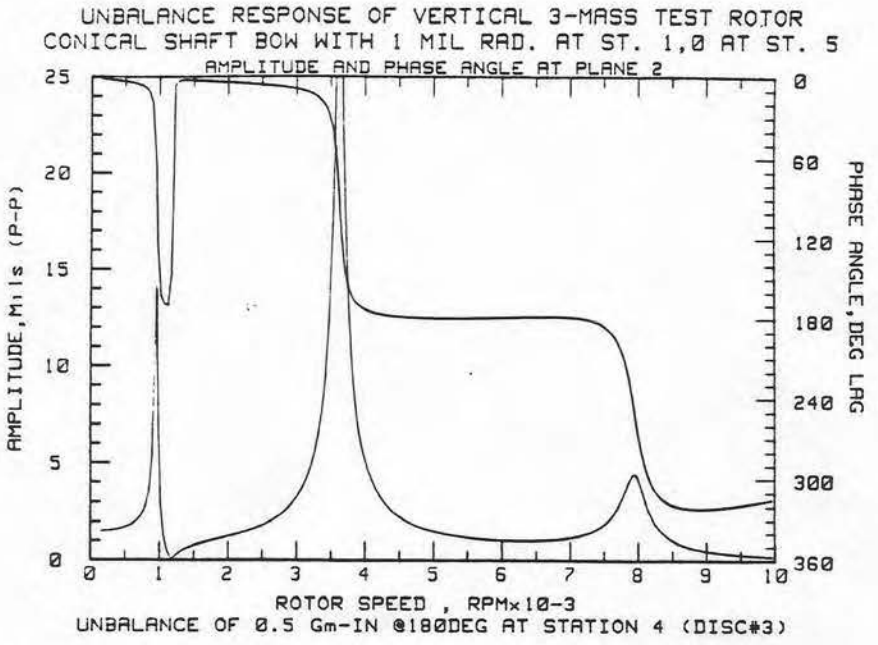

Figure 19. Unbalance Response at Station 2 with Trial Unbalance of 0.5 gm-in at 180 Degrees at Station 4

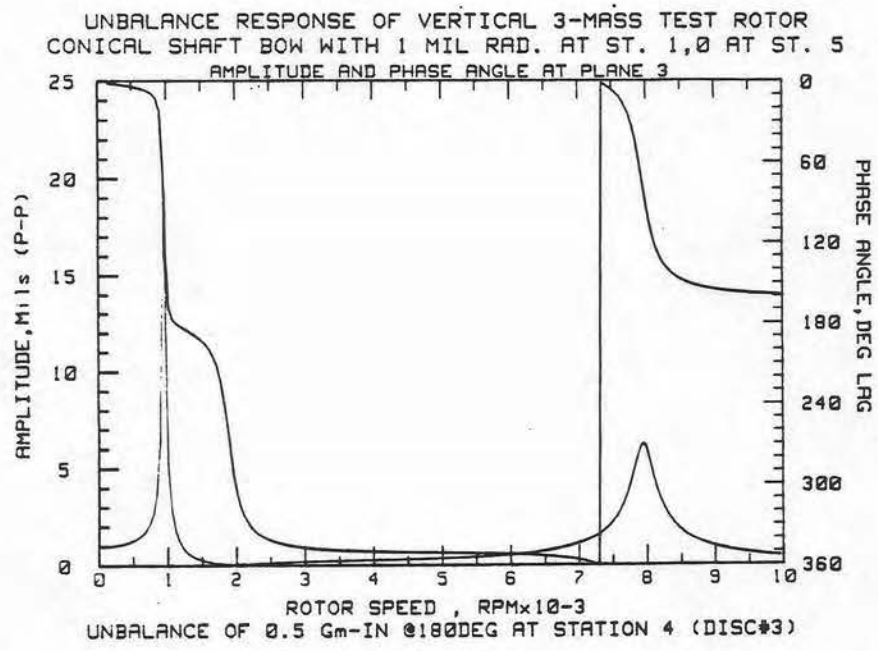

Figure 20. Unbalance Response at Station 3 with Trial Unbalance of 0.5 gm-in at 180 Degrees at Station 4

In this particular example the size of the trial weights, 0.5 gm-in and their location at each balance plane, 180°, were identical. This is not necessary, and in fact, this will seldom be the case.

An important part of the initial measurements is the slowroll vector. This is the runout at the probe locations to be used in balancing taken at a low speed. It should be an indication of shaft bow and mechanical runout.

In general it is impossible to distinguish between true shaft bow and mechanical runout which does not effect the rotor dynamic behavior. For example, the vibration response at any speed may be written as the vector sum of the influence of unbalance (and/or disc skew), shaft bow, and mechanical runout as follows.

$$\{Z\} = [\alpha_u] \{U\} + [\alpha_b] \{Z_b\} + \{Z_r\} \tag{4.4}$$

By application of the trial unbalances at the various stations, the influence matrix $[\alpha_u]$ may be determined. The shaft bow matrix $[\alpha_b]$ may not be determined by the direct application of trial weights.

At low speeds the $[\alpha_u]$ matrix approaches zero while the shaft bow matrix $[\alpha_b]$ approaches the identity matrix. Therefore, at low speeds, the shaft amplitude vector is given by

$$\{Z\} = \{Z_o\} = \{Z_b\} + \{Z_r\} \tag{4.5}$$

When balancing by the influence coefficient method one assumes that the rotor behavior is approximately given by

$$\{Z\} = [\alpha_u] \{U\} + \{Z_o\} + \{\varepsilon\} \tag{4.6}$$

Where $\{\varepsilon\}$ = error function.

The least squared error balancing procedure requires the subtraction of the low speed runout vector and minimizes the system

error. It has been demonstrated by Nicholas, Gunter, and Allaire (2,3), that the subtraction of the low speed runout vector would lead to satisfactory balancing of the Jeffcott rotor. Serious balancing errors may result, however, if the low speed runout is not subtracted from the rotor response.

In this particular balance calculation, the rotor amplitudes and phase angles were recorded at the speeds corresponding to the three critical response speeds of the rotor. While this is theoretically possible to do with a computer program, it is not necessarily possible to perform accurately in practice with a high Q or high amplification factor rotor due to the rapid shift of the phase angles with respect to speed in the critical speed vicinity. Under these circumstances, several speed points in the vicinity of the critical speed should be recorded to insure accuracy.

Table 8 gives the data which was used to balance the rotor using a least squared error influence coefficient technique and a linear programming procedure. The probe locations are listed as disc 1, disc 2, and disc 3, which also happens to be the balance planes. This is not necessary.

Table 8 is a run of the balancing program LINLS. At the bottom of the table the corrective balance weights have been predicted using two different methods. The linear programing technique allows for the trial weight sizes to be constrained where as the least squares method does not. Here no constraint was used in the linear programing solution. As can be seen the two solutions are nearly identical although the algorithms differ immensely.

Table 8

Vertical Three-Mass with Conical Shaft Bow

A. BASE DATA

IDENTIFICATION FOR:

PROBE #1	DISC #1
PROBE #2	DISC #2
PROBE #3	DISC #3

IDENTIFICATION FOR:

PLANE #1	DISC #1
PLANE #2	DISC #2
PLANE #3	DISC #3

SPEED	RPM
1	958
2	3620
3	7960

SLOWROLL

	MILS	DEG LAG
PROBE 1	1.50	0.0
PROBE 2	1.00	0.0
PROBE 3	.50	0.0

INITIAL READINGS:

	MILS	DEG LAG
SPEED 1 PROBE 1	22.30	89.0
SPEED 1 PROBE 2	30.40	91.0
SPEED 1 PROBE 3	22.00	92.0
SPEED 2 PROBE 1	13.90	95.0
SPEED 2 PROBE 2	.30	189.0
SPEED 2 PROBE 3	13.90	276.0
SPEED 3 PROBE 1	3.00	108.0
SPEED 3 PROBE 2	4.40	286.0
SPEED 3 PROBE 3	3.00	103.0

THE TRIAL UNBALANCES:

	MAGNITUDE	DEG LEAD
PLANE 1	.50	180.0
PLANE 2	.50	180.0
PLANE 3	.50	180.0

Table 8 (Continued)

B. THE READINGS AFTER A TRIAL WEIGHT HAS BEEN ADDED TO THE PLANE INDICATED:

	MILS	DEG LAG
PLANE 1 SPEED 1 PROBE 1	14.10	89.0
PLANE 1 SPEED 1 PROBE 2	19.40	92.0
PLANE 1 SPEED 1 PROBE 3	14.00	93.0
PLANE 1 SPEED 2 PROBE 1	3.70	245.0
PLANE 1 SPEED 2 PROBE 2	.30	348.0
PLANE 1 SPEED 2 PROBE 3	4.10	56.0
PLANE 1 SPEED 3 PROBE 1	4.20	271.0
PLANE 1 SPEED 3 PROBE 2	6.20	75.0
PLANE 1 SPEED 3 PROBE 3	4.30	253.0
PLANE 2 SPEED 1 PROBE 1	11.00	89.0
PLANE 2 SPEED 1 PROBE 2	15.20	93.0
PLANE 2 SPEED 1 PROBE 3	11.00	95.0
PLANE 2 SPEED 2 PROBE 1	13.80	93.0
PLANE 2 SPEED 2 PROBE 2	.20	337.0
PLANE 2 SPEED 2 PROBE 3	13.90	279.0
PLANE 2 SPEED 3 PROBE 1	13.10	92.0
PLANE 2 SPEED 3 PROBE 2	19.10	276.0
PLANE 2 SPEED 3 PROBE 3	13.20	91.0
PLANE 3 SPEED 1 PROBE 1	14.10	89.0
PLANE 3 SPEED 1 PROBE 2	19.40	92.0
PLANE 3 SPEED 1 PROBE 3	14.00	94.0
PLANE 3 SPEED 2 PROBE 1	31.00	91.0
PLANE 3 SPEED 2 PROBE 2	.30	348.0
PLANE 3 SPEED 2 PROBE 3	31.00	272.0
PLANE 3 SPEED 3 PROBE 1	4.40	251.0
PLANE 3 SPEED 3 PROBE 2	6.20	75.0
PLANE 3 SPEED 3 PROBE 3	4.20	274.0

C. THE CORRECTION WEIGHTS BY LEAST SQUARED ERROR METHOD:

	MAGNITUDE	DEG (LEAD)
PLANE 1	.605	172.72
PLANE 2	.412	179.22
PLANE 3	.203	178.25

D. THE CORRECTION WEIGHTS BY LINEAR PROGRAMING:

	MAGNITUDE	DEG (LEAD)
PLANE 1	.601	173.31
PLANE 2	.413	179.22
PLANE 3	.203	178.87

THE MAX PREDICTED AMPLITUDE IN ANY X OR Y DIRECTION SHOULD BE < = .182914051946

Table 9

Unbalance Response of Vertical Three-Mass Test
Rotor Conical Shaft Bow with 1 Mil Rad.
at Station 1,0 at Station 5

ORDER OF SYSTEM IS 5

ROTOR UNBALANCE

St. No.	UB (Gm-In)	ANGLE (DEG LAG)
1	0.00	0.0
2	.61	-172.7
3	.41	-179.2
4	.20	-178.3
5	0.00	0.0

SHAFT BOW (MILS, P-P)

St. No.	BOW (MILS)	ANGLE (DEG LAG)
1	2.0000	0
2	1.5000	0
3	1.0000	0
4	.5000	0
5	0.0000	0

ROTOR MAXIMUM AMPLITUDES OF MOTION-
UNCOMPENSATED AND COMPENSATED:

St. No.	x (MILS) (P-P)	Phase Deg Lag	Nrpm	Xc (MILS) (P-P)	Phasec Deg Lag	Nrpm	Ac (Dim)
1	2.02	8.5	3,610	.73	109.6	9,950	.2
2	1.60	4.4	3,615	.30	152.7	956	23.4
3	1.02	4.1	7,700	.40	160.5	957	24.6
4	.54	358.0	8,050	.29	164.8	958	24.9
5	.05	314.2	7,955	.05	314.2	7,955	22.6

Table 10

Balancing Prediction Using First Critical Speed Data

	MAGNITUDE	DEG LEAD
PLANE 1	.50	180.0
PLANE 2	.50	180.0
PLANE 3	.50	180.0

THE READINGS AFTER A TRIAL WEIGHT HAS BEEN ADDED TO THE PLANE INDICATED:

	MILS	DEG LAG
PLANE 1 SPEED 1 PROBE 1	14.10	89.0
PLANE 1 SPEED 1 PROBE 2	19.40	92.0
PLANE 1 SPEED 1 PROBE 3	14.00	93.0
PLANE 2 SPEED 1 PROBE 1	11.00	89.0
PLANE 2 SPEED 1 PROBE 2	15.20	93.0
PLANE 2 SPEED 1 PROBE 3	11.00	95.0
PLANE 3 SPEED 1 PROBE 1	14.10	89.0
PLANE 3 SPEED 1 PROBE 2	19.40	92.0
PLANE 3 SPEED 1 PROBE 3	14.00	94.0

THE CORRECTION WEIGHTS BY LEAST SQUARED ERROR METHOD:

	MAGNITUDE	DEG (LEAD)
PLANE 1	1.364	270.20
PLANE 2	3.015	137.36
PLANE 3	2.172	321.26

THE CORRECTION WEIGHTS BY LINEAR PROGRAMING:

	MAGNITUDE	DEG (LEAD)
PLANE 1	1.364	270.20
PLANE 2	3.015	137.36
PLANE 3	2.172	321.26

THE RUNOUT IN ANY X OR Y DIRECTION SHOULD BE < = 0

Figures 21 through 25 show the results of the balancing. In each of the figures the amplitude at each speed is roughly equal to the initial bow, indicating that there is little bending of the shaft occurring. In Figure 25, plane 5 data, the amplitude follows the speed axis. Table 9 summarizes the run of the ROTOR program which produced Figures 21 through 25.

The figures demonstrate that if accurate data can be obtained at or near the three critical speeds, then the rotor may be accurately balanced through all the critical speeds by means of the least squared error procedure. Note that the final correction distribution is not exactly out of phase to the shaft bow, but is slightly leading by several degrees. It will be shown that this balancing distribution is close to the static unbalance offset of the discs. With a completely undamped system, the balance distribution would be at exactly 180°.

A completely different balancing distribution is obtained if one only uses the data obtained near, for example, the rotor first critical speed. Table 10 represents the balancing calculations using only the data at the first critical speed. The balance correction weights given by Table 10 are 1.3, 3,0 and 2.17 gm-in at phase lead angles of 270, 137 and 321 degrees. These values will accurately balance the first mode, but will completely upset the second and third critical speeds. In general, it is seen that a high Q rotor may not be accurately balanced by the exact point influence coefficient method. In order to accurately balance this class of rotor by the influence coefficient method, the least squared error or linear programming method must be used. The least squared error method reduces to the exact point method when only one speed case is employed.

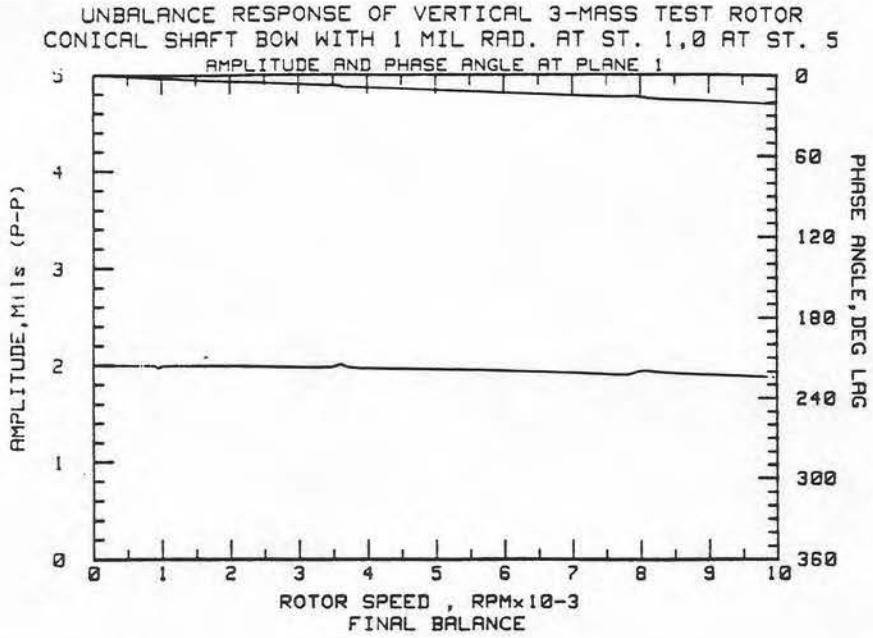

Figure 21. Unbalance Response at Station 1 with Corrective Balance Weights

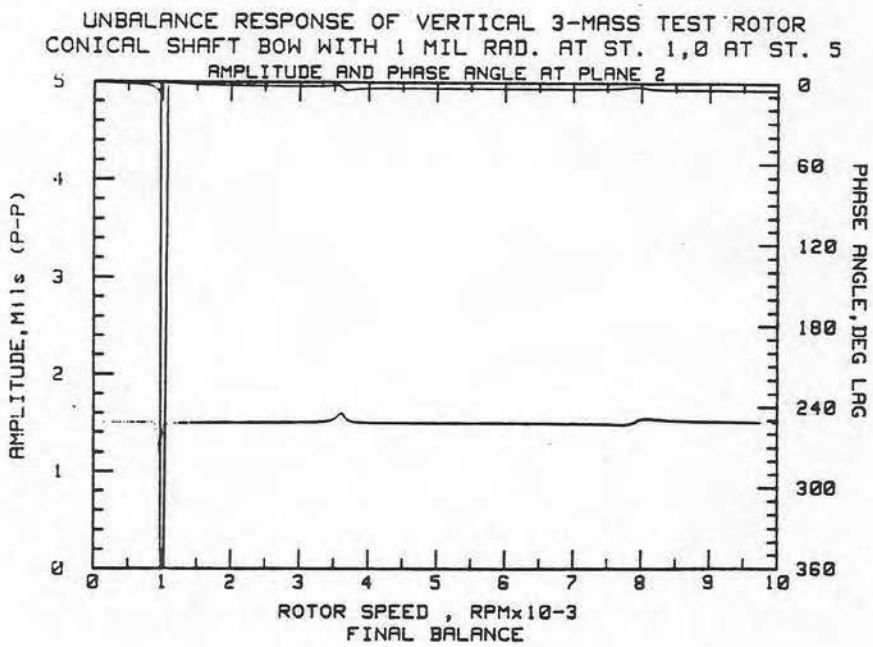

Figure 22. Unbalance Response at Station 2 with Corrective Balance Weights

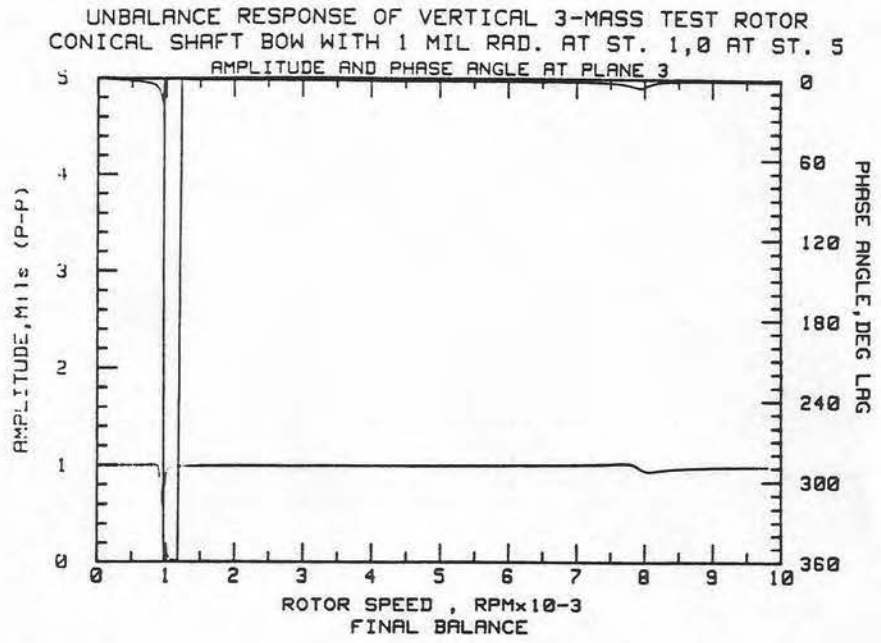

Figure 23. Unbalance Response at Station 3 with Corrective Balance Weights

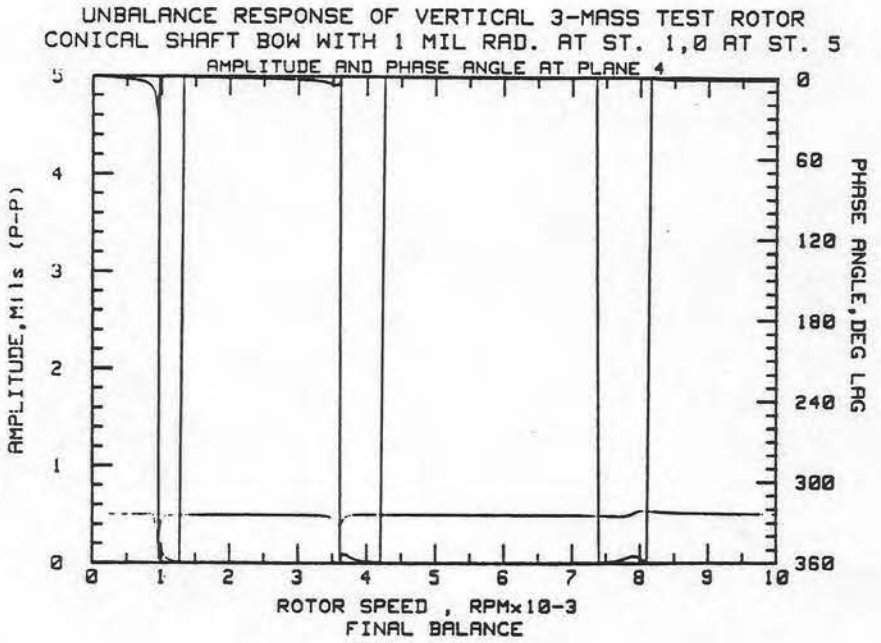

Figure 24. Unbalance Response at Station 4 with Corrective Balance Weights

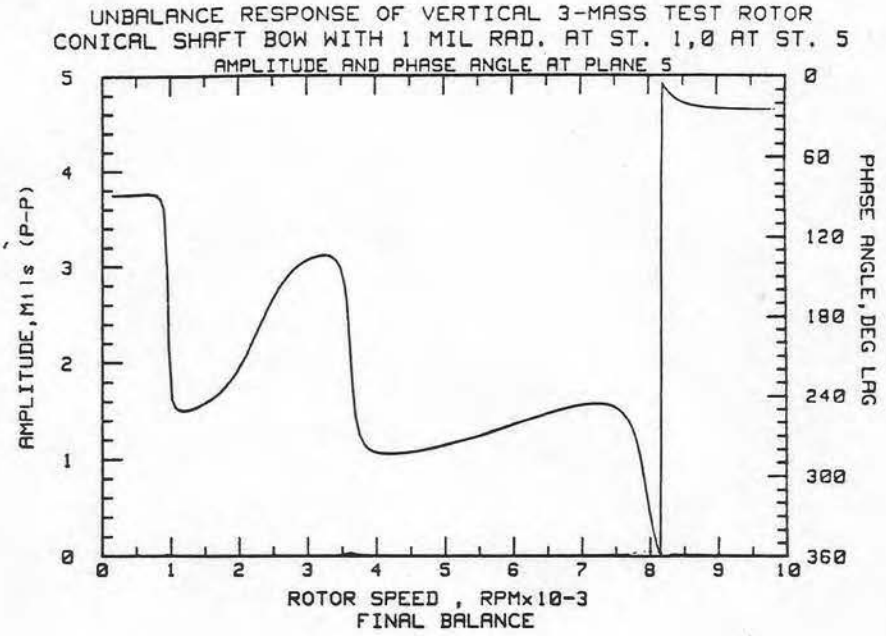

Figure 25. Unbalance Response at Station 5 with Corrective Balance Weights

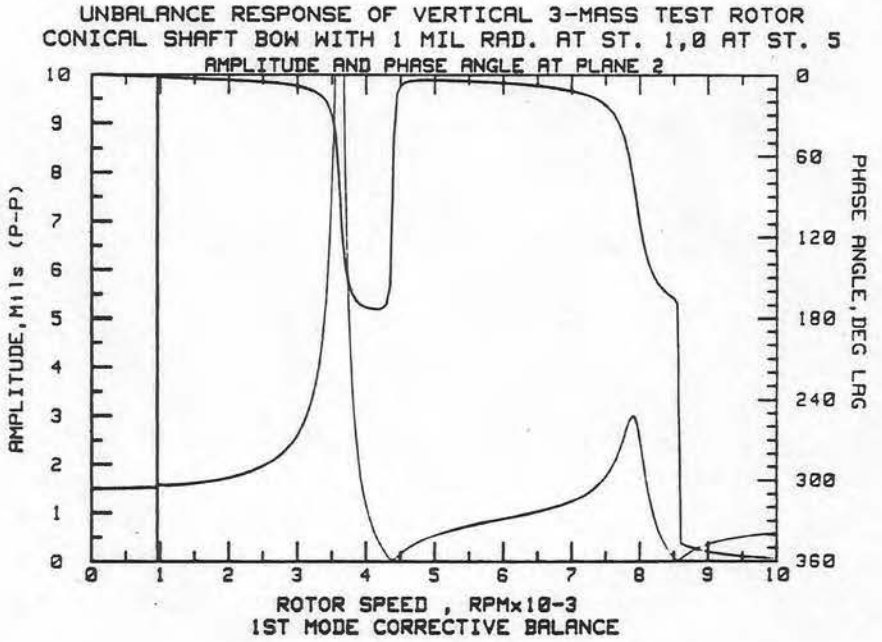

Figure 26. Unbalance Response at Station 2 with a First Mode Correction

4.2 Modal Balancing

Next the original rotor, Figures 10 through 14, is balanced using modally distributed weights. An approximate first mode distribution of 0.73 gm-in was added to disc 1, 1.00 gm-in to disc 2, and 0.73 gm-in to disc 3. All weights were placed 180° out of phase to the shaft bow. The rotor unbalance response was calculated with the first mode unbalance distribution added to the system. The data at the first critical speed is summarized in Table 11.

Table 11 also presents a first mode corrective balance. In order to calculate the actual first mode correction we note that the trial weight was given as a relative magnitude of 1 and phase of 0. The corrective balance is predicted to have a relative magnitude of 0.48 and phase of 355.46°. The first mode correction will have magnitudes of $0.73 \times 0.488 = 0.35$ gm-in at disc 1 and disc 3. Disc 2 will have magnitude $1 \times 0.488 = 0.49$ gm-in. The phase angle for each plane will be $180° + 355.46° = 175.5°$ lead angle or $360° - 175.5° = 184.5°$ lag angle. As always care must be taken to ensure the proper angles are used. Lead angles are measured in the direction of rotation. Lag angles are measured against the direction of rotation.

Figures 26 through 29 show the results of adding a corrective balance of 0.35 gm-in to disc 1 and disc 3, and adding 0.49 gm-in to disc 2 at a 175.5 lead angle. It can be seen that this corrective balance has little influence on the second and third critical speeds, while it essentially eliminates any response at the first critical speed.

Table 11

Vertical Three-Mass with Conical Shaft Bow

IDENTIFICATION FOR:

PROBE #1
PROBE #2
PROBE #3

IDENTIFICATION FOR:

PLANE #1 1st Mode Balance Weight

SPEED	RPM
1	958

SLOWROLL

	MILS	DEG LAG
PROBE 1	1.50	0.0
PROBE 2	1.00	0.0
PROBE 3	.50	0.0

INITIAL READINGS:

	MILS	DEG LAG
SPEED 1 PROBE 1	22.30	89.0
SPEED 1 PROBE 2	30.40	91.0
SPEED 1 PROBE 3	22.00	92.0

THE TRIAL UNBALANCES:

	MAGNITUDE	DEG LEAD
PLANE 1	1.00	0.0

THE READINGS AFTER A TRIAL WEIGHT HAS BEEN ADDED TO THE PLANE INDICATED:

	MILS	DEG LAG
PLANE 1 SPEED 1 PROBE 1	23.17	268.0
PLANE 1 SPEED 1 PROBE 2	32.11	266.0
PLANE 1 SPEED 1 PROBE 3	23.29	265.0

THE CORRECTION WEIGHTS BY LEAST SQUARED ERROR METHOD:

	MAGNITUDE	DEG (LEAD)
PLANE 1	.488	355.46

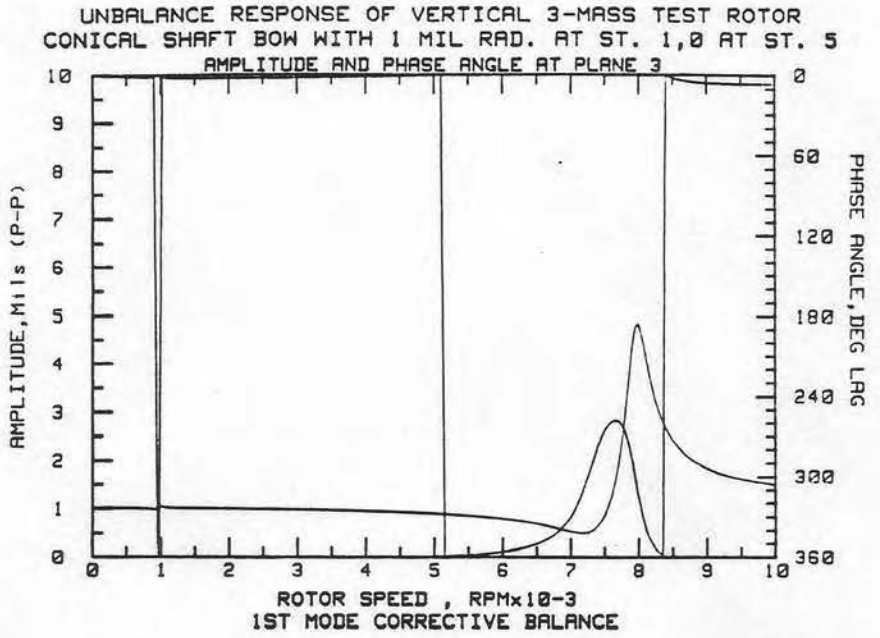

Figure 27. Unbalance Response at Station 3 with a First Mode Correction

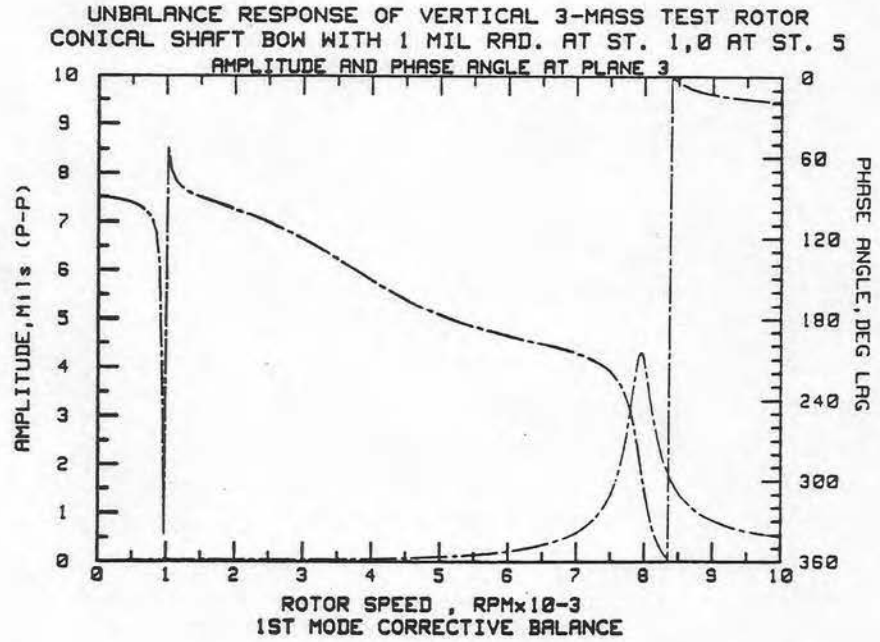

Figure 28. Compensated Response at Station 3 with a First Mode Correction

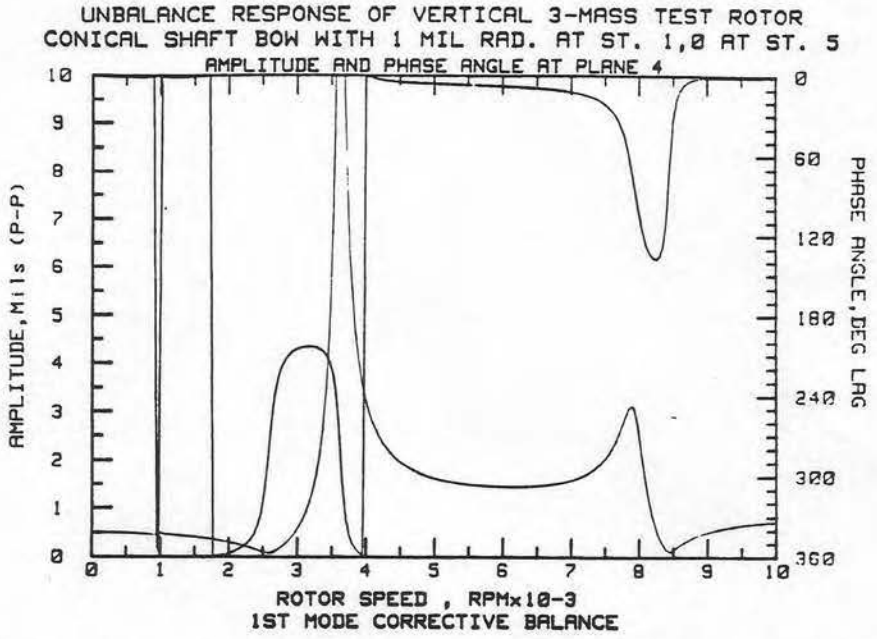

Figure 29. Unbalance Response at Station 3 with a First Mode Correction

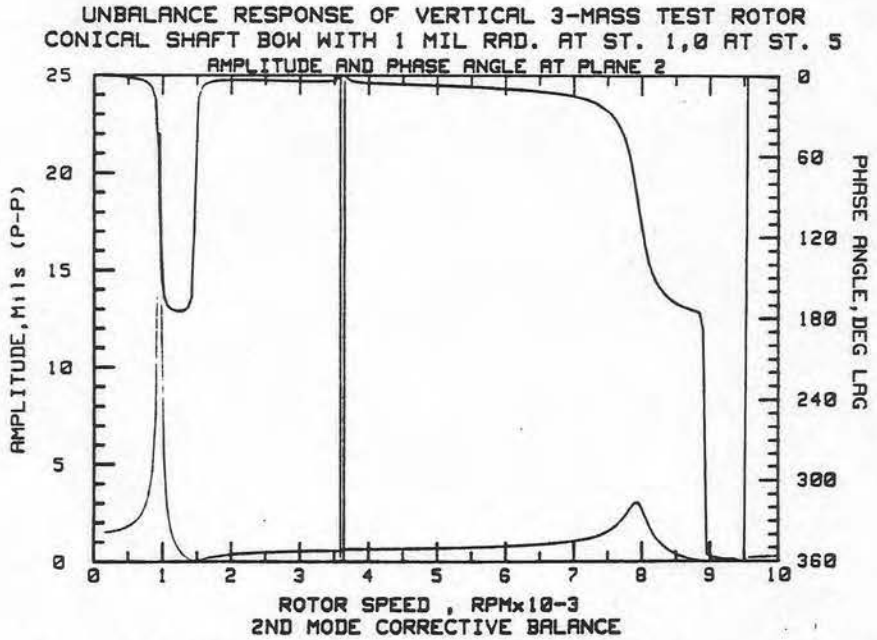

Figure 30. Unbalance Response at Station 2 with Second Mode Correction

Similar to the first mode balancing, a second mode trial weight of 1 gm-in at 180° to disc 1 and 1 gm-in at 0° to disc 3, no weight is added to disc 2.

Table 12 summarizes the results at the second critical speed as well as computing a corrective weight. Table 12 also points out the fact that this trial weight caused severe vibration problems. This should be avoided where possible on actual machinery.

The corrective balance for each plane is predicted to be 0.20 at a phase of 350.4° lead angle. This translates to the following corrective balances.

<u>at Disc 1</u>		
magnitude	1 x 0.20	= 0.20 gm-in
phase	180° + 350.4°	= 170.4° lead
		= 189.6° lag
<u>at Disc 2</u>		
magnitude	1 x 0.20	= 0.20 gm-in
phase	0° + 350.4°	= 350.4° lead
		= 9.6° lag

This weight distribution was applied to the rotor. The results are shown in Figures 6.30 and 6.31. No data from plane 3 is shown since this is a node for the second critical speed. The second critical speed seems to have been removed in Figures 6.30 and 6.31; but neither the first critical speed nor the third critical speed has been significantly altered.

Next a third mode distribution is added to the rotor. The individual weights were:

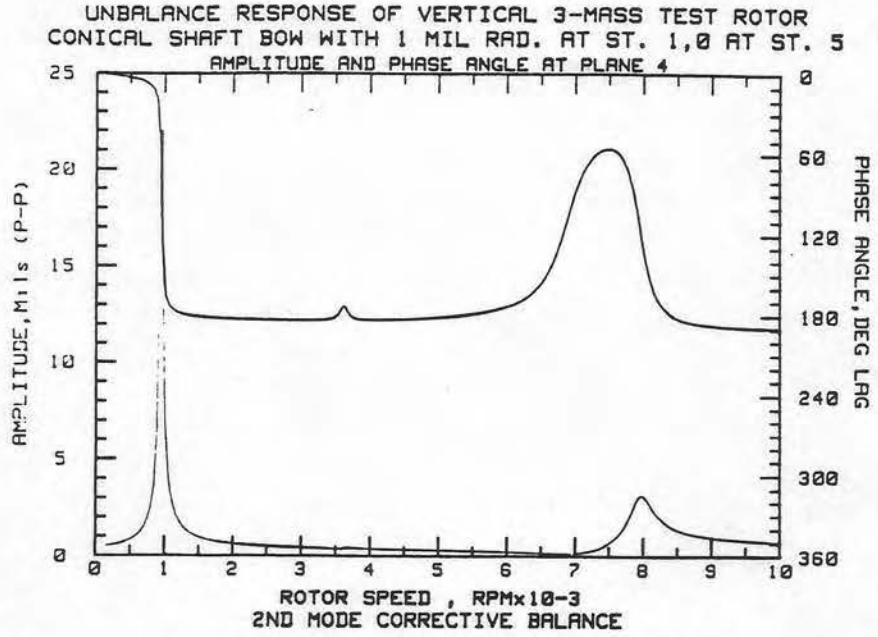

Figure 31. Unbalance Response at Station 4 with Second Mode Correction

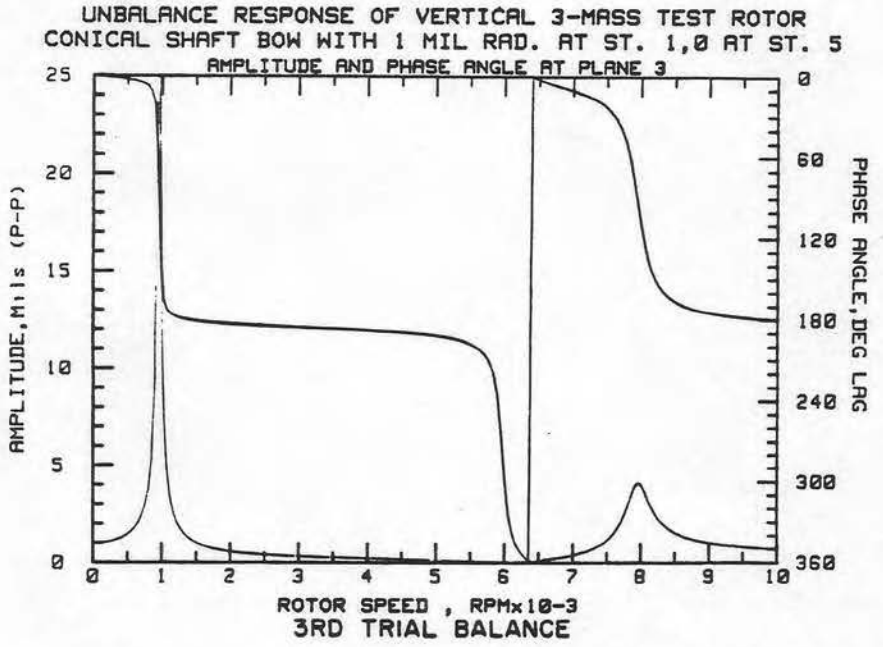

Figure 32. Unbalance Response at Station 3 with a Trial Third Mode Distribution

Table 12

Vertical Three-Mass with Conical Shaft Bow

IDENTIFICATION FOR:

PROBE #1
PROBE #2
PROBE #3

IDENTIFICATION FOR:

PLANE #1 2nd Mode Balance Weight

SPEED	RPM
1	3620

SLOWROLL

	MILS	DEG LAG
PROBE 1	1.50	0.0
PROBE 2	1.00	0.0
PROBE 3	.50	0.0

INITIAL READINGS:

	MILS	DEG LAG
SPEED 1 PROBE 1	13.90	95.0
SPEED 1 PROBE 2	.30	189.0
SPEED 1 PROBE 3	13.90	276.0

THE TRIAL UNBALANCES:

	MAGNITUDE	DEG LEAD
PLANE 1	1.00	0.0

THE READINGS AFTER A TRIAL WEIGHT HAS BEEN ADDED TO THE PLANE INDICATED:

	MILS	DEG LAG
PLANE 1 SPEED 1 PROBE 1	54.98	266.0
PLANE 1 SPEED 1 PROBE 2	.33	189.0
PLANE 1 SPEED 1 PROBE 3	55.02	86.0

THE CORRECTION WEIGHTS BY LEAST SQUARED ERROR METHOD:

	MAGNITUDE	DEG (LEAD)
PLANE 1	.203	350.37

	Magnitude	Phase
Disc 1	.068	0° lead = 0° lag
Disc 2	.100	180° lead = 180° lag
Disc 3	.068	0° lead = 0° lag

Figure 32 shows the results of this trial weight. This figure shows that this distribution has little effect on the first two critical speeds while it reduces the third critical speed.

LINLS was run and a third mode correction was predicted:

	Magnitude	Phase
Disc 1	.100	170.2° lead = -170.2° lag
Disc 2	.150	-9.8° lead = 9.8° lag
Disc 3	.068	170.2° lead = -170.2° lag

Table 13 shows the run of LINLS. Figures 33 through 35 show the results of the corrective balance for the third mode. The first two modes are relatively unchanged while the third mode is corrected.

Table 13 contains the data from the modal unbalances. It also predicts the corrective balance weights.

To compute the correction weights for each disc first multiply the first mode weights by .429 and add 356.60° to the phase to get.

	Magnitude	Phase
Disc 1	.311	176.6° lead = 183.4° lag
Disc 2	.429	176.6° lead = 183.4° lag
Disc 3	.311	176.6° lead = 183.4° lag

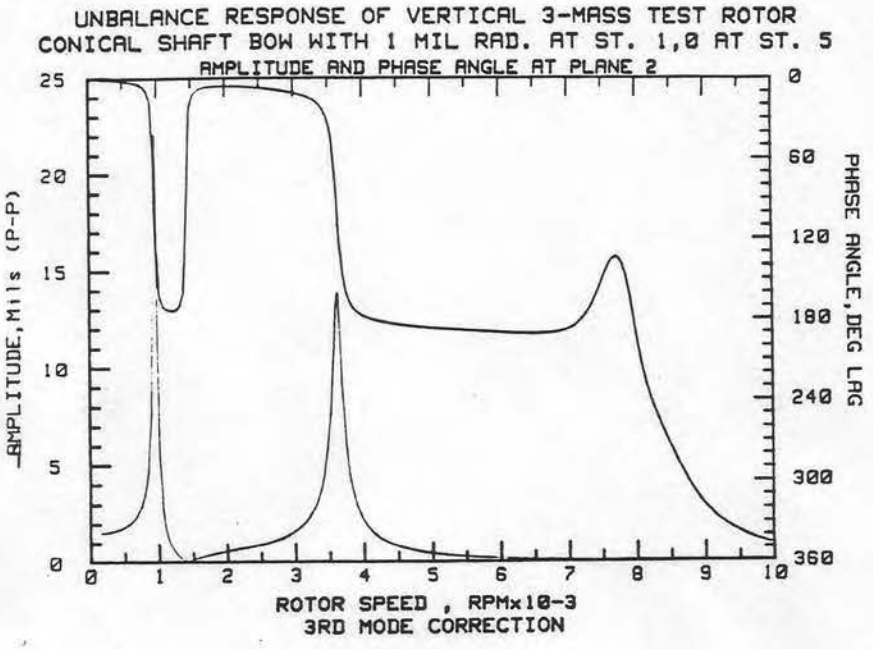

Figure 33. Unbalance Response at Station 2 with Third Mode Correction

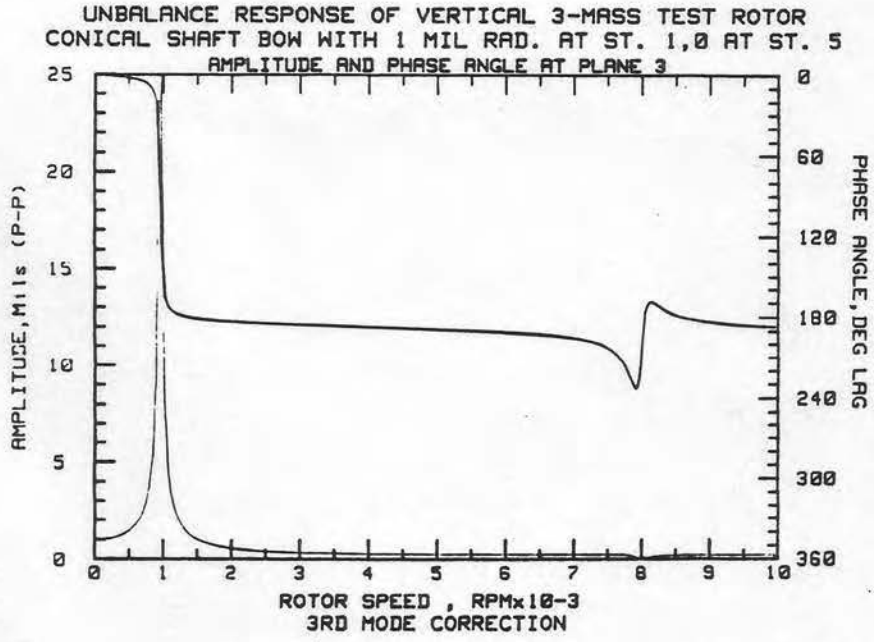

Figure 34. Unbalance Response at Station 3 with Third Mode Correction

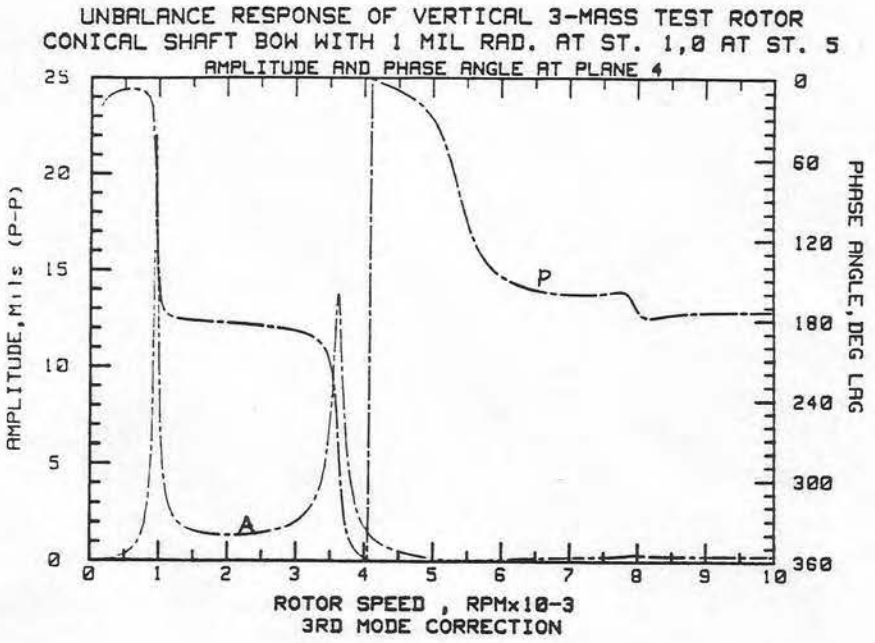

Figure 35. Compensated Response at Station 4 with Third Mode Correction

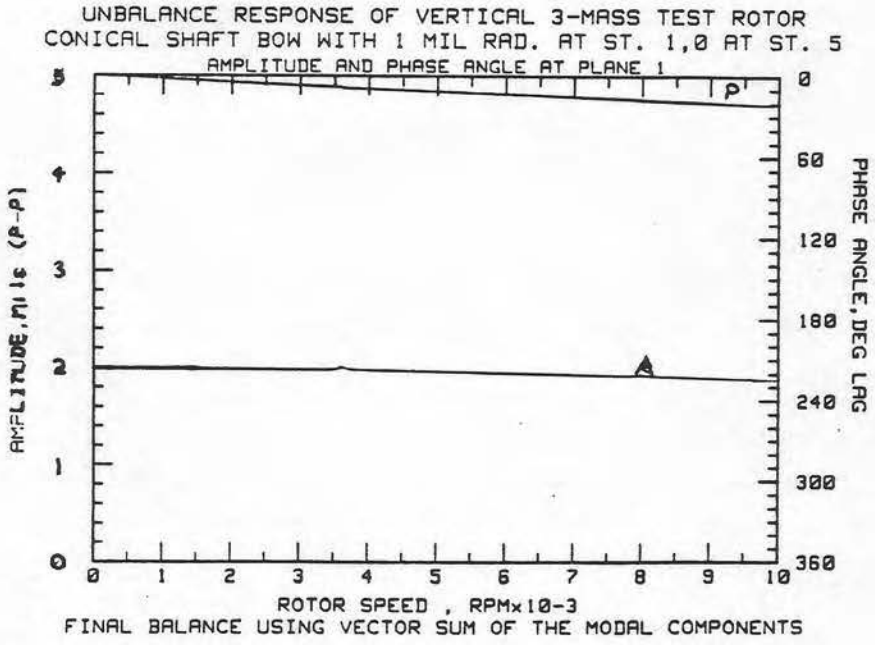

Figure 36. Unbalance Response at Station 1 with the Three Modal Corrections

Table 13

Vertical Three-Mass with Conical Shaft Bow

IDENTIFICATION FOR:

PROBE #1	DISC #1
PROBE #2	DISC #2
PROBE #3	DISC #3

IDENTIFICATION FOR:

PLANE #1	1st Mode Unbalance
PLANE #2	2nd Mode Unbalance
PLANE #3	3rd Mode Unbalance

SPEED	RPM
1	958
2	3620
3	7960

SLOWROLL

	MILS	DEG LAG
PROBE 1	1.50	0.0
PROBE 2	1.00	0.0
PROBE 3	.50	0.0

INITIAL READINGS:

	MILS	DEG LAG
SPEED 1 PROBE 1	22.30	89.0
SPEED 1 PROBE 2	30.40	91.0
SPEED 1 PROBE 3	22.00	92.0
SPEED 2 PROBE 1	13.90	95.0
SPEED 2 PROBE 2	.30	189.0
SPEED 2 PROBE 3	13.90	276.0
SPEED 3 PROBE 1	3.00	108.0
SPEED 3 PROBE 2	4.40	286.0
SPEED 3 PROBE 3	3.00	103.0

THE TRIAL UNBALANCES:

	MAGNITUDE	DEG LEAD
PLANE 1	1.00	0.0
PLANE 2	1.00	0.0
PLANE 3	1.00	0.0

Table 13 (Continued)

THE READINGS AFTER A TRIAL WEIGHT HAS BEEN ADDED TO THE PLANE INDICATED:

	MILS	DEG LAG
PLANE 1 SPEED 1 PROBE 1	23.17	268.0
PLANE 1 SPEED 1 PROBE 2	32.11	266.0
PLANE 1 SPEED 1 PROBE 3	23.29	265.0
PLANE 1 SPEED 2 PROBE 1	13.80	87.0
PLANE 1 SPEED 2 PROBE 2	2.32	358.0
PLANE 1 SPEED 2 PROBE 3	14.21	284.0
PLANE 1 SPEED 3 PROBE 1	2.74	78.0
PLANE 1 SPEED 3 PROBE 2	5.71	316.0
PLANE 1 SPEED 3 PROBE 3	2.87	74.0
PLANE 2 SPEED 1 PROBE 1	22.03	89.0
PLANE 2 SPEED 1 PROBE 2	30.38	91.0
PLANE 2 SPEED 1 PROBE 3	21.99	91.0
PLANE 2 SPEED 2 PROBE 1	54.98	266.0
PLANE 2 SPEED 2 PROBE 2	.33	189.0
PLANE 2 SPEED 2 PROBE 3	55.02	86.0
PLANE 2 SPEED 3 PROBE 1	3.41	54.0
PLANE 2 SPEED 3 PROBE 2	4.37	289.0
PLANE 2 SPEED 3 PROBE 3	4.95	143.0
PLANE 3 SPEED 1 PROBE 1	24.01	89.0
PLANE 3 SPEED 1 PROBE 2	33.10	91.0
PLANE 3 SPEED 1 PROBE 3	23.96	91.0
PLANE 3 SPEED 2 PROBE 1	13.87	96.0
PLANE 3 SPEED 2 PROBE 2	.48	186.0
PLANE 3 SPEED 2 PROBE 3	13.85	276.0
PLANE 3 SPEED 3 PROBE 1	5.14	105.0
PLANE 3 SPEED 3 PROBE 2	7.39	282.0
PLANE 3 SPEED 3 PROBE 3	5.15	102.0

THE CORRECTION WEIGHTS BY LEAST SQUARED ERROR METHOD:

	MAGNITUDE	DEG (LEAD)
PLANE 1	.429	356.60
PLANE 2	.204	350.96
PLANE 3	1.413	166.86

THE CORRECTION WEIGHTS BY LINEAR PROGRAMING:

	MAGNITUDE	DEG (LEAD)
PLANE 1	.435	356.07
PLANE 2	.207	351.96
PLANE 3	1.284	168.60

THE RUNOUT IN ANY X OR Y DIRECTION SHOULD BE < = .331624109853

The second mode

	Magnitude	Phase		
Disc 1	0.20	171.0° lead	=	189.0° lag
Disc 2	0	0° lead		
Disc 3	0.20	351° lead	=	9° lag

The third mode

	Magnitude	Phase		
Disc 1	0.10	356.6° lead	=	3.4° lag
Disc 2	0.14	176.6° lead	=	183.4° lag
Disc 3	0.10	356.6° lead	=	3.4° lag

The vector sum of these weights yields the final corrective balance using modal techniques.

Final Modal Balance

	Magnitude	Phase		
Disc 1	0.61	172.4° lead	=	187.6° lag
Disc 2	0.42	178.5° lead	=	181.5° lag
Disc 3	0.20	177.2° lead	=	182.8° lag

These numbers are very close to those computed by the first method of balancing (see Table 9).

Figures 36 through 41 show the results of the modal balance which is very similar to the first balance.

This example points out an advantage of adding distributed trial weights as opposed to adding individual trial weights. With distributed modal trial weights, one critical speed may be balanced without great influence to the other critical speeds. When adding individual

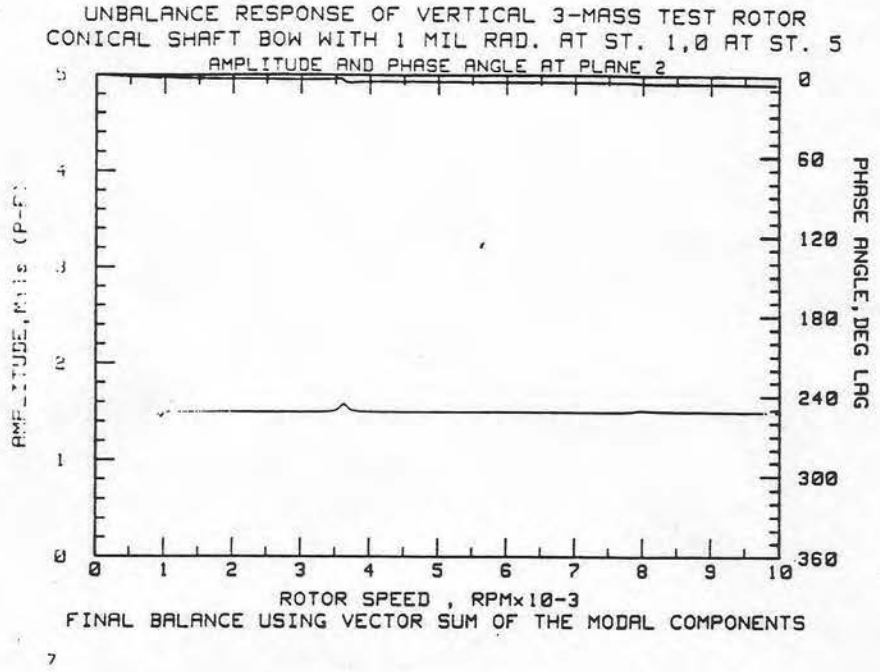

Figure 37. Unbalance Response at Station 2 with the Three Modal Corrections

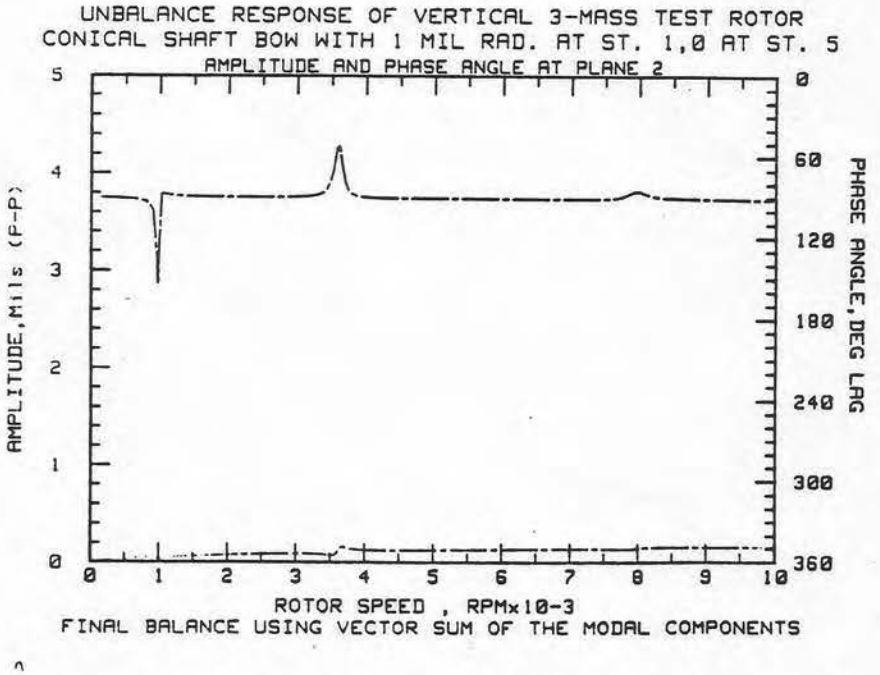

Figure 38. Compensated Response at Station 2 with the Three Modal Corrections

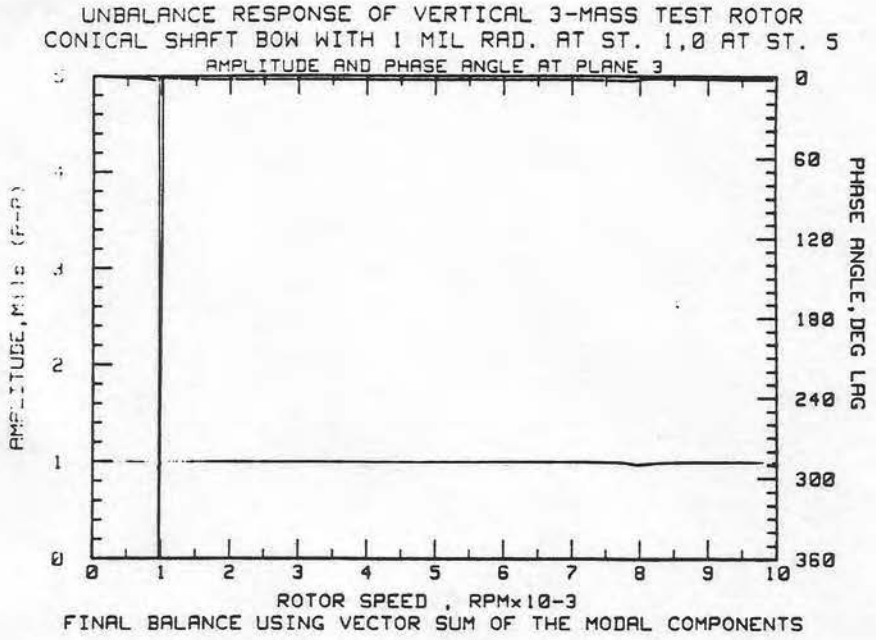

Figure 39. Unbalance Response at Station 3 with the Three Modal Corrections

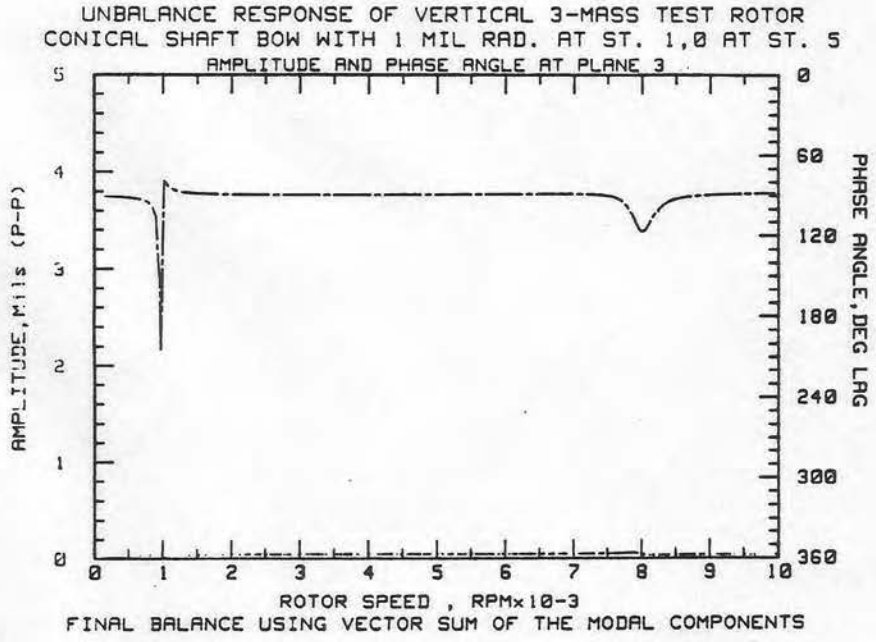

Figure 40. Compensated Response at Station 3 with the Three Modal Corrections

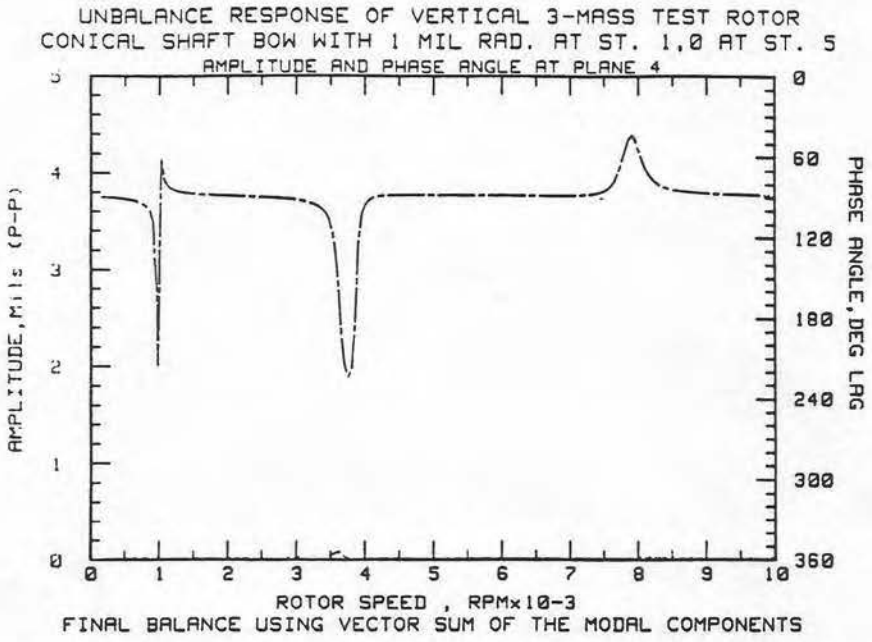

Figure 41. Compensated Response at Station 4 with the Three Modal Corrections

weights some critical speeds may be adversely affected so that the rc cannot be safely run up to the desired speed needed to gather da

Also, this rotor system cannot be balanced by the exact po method. Table 10 gives the results for an exact point balance at t first critical speed. When these weights are added the predicted r sponse exceeds 158 mils at the third critical, while balancing the fir critical speed very well. The exact point method cannot be employed balance the third critical speed without upsetting the first mode balanc

REFERENCES

1. Gunter, E. J., Springer, H., and Humphris, R. R., "Dynamic Unbalance Response and Stability Characteristics of a Vertical Three-Mass Rotor-Bearing System. Part I: Balancing of a Multi Mass Flexible Rotor Bearing System Without Phase," Report No. UVA/643078/MAE81/106, University of Virginia (December 1981).

2. Nicholas, J. C., Gunter, E. J., and Allaire, P. E., "Effect of Residual Shaft Bow on Unbalance Response and Balancing of a Single Mass Flexible Rotor. Part I: Unbalance Response," ASME Transactions, Journal of Engineering for Power, Vol. 98, Series A, No. 2 (April 1976), pp. 171-81.

3. Nicholas, J. C., Gunter, E. J., and Allaire, P. E., "Effect of Residual Shaft Bow on Unbalance Response and Balancing of a Single Mass Flexible Rotor. Part II: Balancing," ASME Transactions, Journal of Engineering for Power, Vol. 98, Series A, No. 2 (April 1976), pp. 182-89.

4. Gunter, E. J., Barrett, L. E., and Allaire, P. E., "Balancing of Multimass Flexible Rotors. Part I: Theory," Proceedings of the Fifth Turbomachinery Symposium (Texas A & M University, October 1976).

5. Gunter, E. J., Barrett, L. E., and Allaire, P. E., "Balancing of Multimass Flexible Rotors. Part II: Experimental Results," Proceedings of the Fifth Turbomachinery Symposium (Texas A & M University, October 1976).

6. Little, R. M., and Pilkey, W. D., "A Linear Programming Approach for Balancing Flexible Rotors," Journal of Engineering for Industry, Vol. 98, Series B, No. 3 (August 1976).

7. Palazzolo, A. B., and Gunter, E. J., "A Multimass Flexible Rotor Balancing by the Least Squares Error Method - A Manual for Use with the Computer Program LTSQAP," Report No. UVA/464761/MAE77/161, University of Virginia (August 1977), 65 pp.

8. Gunter, E. J. (ed.), "Selected Papers on Field Balancing of Rotating Machinery - Advanced Theory and Techniques," Report No. UVA/464761/MAE78/149, University of Virginia (March 1978), 188 pp.

9. Rooke, J., Flack, R. D., and Gunter, E. J., "The Influence of Residual Shaft Bow and Run Out on the Unbalance Response of the Jeffcott Rotor," Report No. UVA/464761/MAE80/158, University of Virginia (May 1980), 284 pp.

10. Woomer, E., and Pilkey, W. D., "The Balancing of Rotating Shafts by Quadratic Programming," Journal of Mechanical Design (1980).

APPENDIX A

The general rotor equations of motion including shaft bow are given by

$$[M]\{\ddot{X}\} + [C]\{\ddot{X}\} + [K]\{X\} = [K]\{X\}_b + F(t) \qquad A1$$

It is assumed that acceleration is negligible and the external forcing function is of the form

$$F_i(t) = \omega^2 \{U \cos(\omega t - \phi_u)\};$$

where ϕ_u = lag angle of unbalance from the timing mark

$$= \omega^2[U_x \cos \omega t + U_y \sin \omega t];$$

where

$$U_x = U \cos \phi_u,\ U_y = U \sin \phi_u$$

The rotor amplitude X and the shaft bow X_b may be expressed as

$$X = X_c \cos t\ \omega t + X_s \sin \omega t \qquad A.2$$

$$\dot{X} = -\omega X_c \sin \omega t + \omega X_s \cos \omega t \qquad A.3$$

$$\ddot{X} = -\omega^2 X_c \cos \omega t - \omega^1 X_s \sin \omega t \qquad A.4$$

The matrix equations of motion in terms of the in phase and out of phase shaft components $\{X_c\}$ and $\{X_s\}$ may be expressed as follows

$$-\omega^2 \begin{bmatrix} M & 0 \\ 0 & M \end{bmatrix} \begin{Bmatrix} X_c \\ Xs \end{Bmatrix} + \omega \begin{bmatrix} 0 & C \\ -C & 0 \end{bmatrix} \begin{Bmatrix} X_c \\ X_s \end{Bmatrix}$$

$$+ \begin{bmatrix} K & 0 \\ 0 & K \end{bmatrix} \begin{Bmatrix} X_c \\ X_s \end{Bmatrix} = \omega^2 \begin{Bmatrix} U_x \\ U_y \end{Bmatrix} + \begin{bmatrix} K & \\ & K \end{bmatrix} \begin{Bmatrix} X_c \\ X_s \end{Bmatrix}_b \qquad A.5$$

See above equation is of order 2N for the solution of the complete displacement vector {X}. Let

$$K = [K] - \omega^2 [M]$$

Let

$$C = \omega[C]$$

$$\{R\} = \omega^2 \begin{Bmatrix} U_x \\ U_y \end{Bmatrix} + \begin{bmatrix} K & 0 \\ 0 & K \end{bmatrix} \begin{Bmatrix} X_c \\ X_b \end{Bmatrix}_b$$

The algebraic equations of motion are given by

$$\begin{bmatrix} K & C \\ -C & K \end{bmatrix} \begin{Bmatrix} X_c \\ X_s \end{Bmatrix} = \begin{Bmatrix} R_1 \\ R_2 \end{Bmatrix} \qquad \text{A.6}$$

The synchronous motion is given by

$$\{X\} = [B] \{R\}$$

Where

$$[B] = \begin{bmatrix} K & C \\ -C & K \end{bmatrix}^{-1}$$

Rather than directly invert the 2N x 2N matrix, the symmetry of the system and matrix partioning will be utilized to reduce the order of the system.

Consider the following:

$$\begin{bmatrix} K & C \\ -C & K \end{bmatrix} \cdot \begin{bmatrix} B_{11} & B_{12} \\ B_{21} & B_{22} \end{bmatrix} = \begin{bmatrix} I & 0 \\ 0 & I \end{bmatrix}$$

Expanding out results in the following equations:

$$KB_{11} + CB_{21} = I \qquad \text{A8.1}$$

$$KB_{12} + CB_{22} = 0 \qquad \text{A8.2}$$

$$- CB_{11} + KB_{21} = 0 \qquad \text{A8.3}$$

$$- CB_{12} + KB_{22} = I \qquad \text{A8.4}$$

Solving for the submatrices Biy yields

$$B_{11} = B_{22} = [K + CK^{-1} C]^{-1} = B \qquad \text{A8.5}$$

$$B_{21} = - B_{12} = K^{-1} C B_{11} = D \qquad \text{A8.6}$$

The unbalance response solution is given by

$$\begin{Bmatrix} X_c \\ x_s \end{Bmatrix} = \begin{bmatrix} B & -D \\ D & B \end{bmatrix} \left[\omega^2 \begin{Bmatrix} U_x \\ U_y \end{Bmatrix} + \begin{bmatrix} K & 0 \\ 0 & K \end{bmatrix} \begin{Bmatrix} X_c \\ X_s \end{Bmatrix}_b \right]$$

$$X_c = [B] \{R_1\} - [D] \{R_2\}$$
$$X_s = [D] \{R_1\} - [B] \{R_2\} \qquad \text{A9}$$

The rotor amplitude phase lag is given by

$$\{\phi\}_i = \tan^{-1} \left(\frac{X_s}{X_c}\right) \qquad \text{A10}$$

APPENDIX B

BALANCING THEORY

I. Least Squares Error Method

The superposition method will be used to set up the equations for the least squares error method. Let

$$A = \begin{bmatrix} a_{11} & a_{12} \cdots\cdots a_{1M} \\ a_{21} & a_{22} \cdots\cdots a_{2M} \\ . & . \quad\quad . \\ . & . \quad\quad . \\ a_{NM} & a_{N2} \cdots\cdots a_{NM} \end{bmatrix}$$ = Influence Coefficients

Let

$$E = \begin{Bmatrix} e_1 \\ e_2 \\ . \\ . \\ . \\ e_N \end{Bmatrix}$$ = initial runout vector - slow roll

$$T = \begin{Bmatrix} T_1 \\ \cdot \\ \cdot \\ \cdot \\ \cdot \\ T_M \end{Bmatrix}$$ = unbalance to be added to rotor to correct initial runout

$$R = \begin{Bmatrix} r_1 \\ r_2 \\ \cdot \\ \cdot \\ \cdot \\ r_N \end{Bmatrix}$$ = runout after adding corrective balances

The basis to the balancing problem is

$$\begin{Bmatrix} r_1 \\ r_2 \\ \cdot \\ \cdot \\ \cdot \\ r_N \end{Bmatrix} = \begin{Bmatrix} e_1 \\ e_2 \\ \cdot \\ \cdot \\ \cdot \\ e_N \end{Bmatrix} + \begin{bmatrix} a_{11} \cdots a_{12} \cdots a_{1M} \\ a_{21} \cdots a_{22} \cdots a_{2M} \\ \cdot \quad\quad \cdot \quad\quad \cdot \\ \cdot \quad\quad \cdot \quad\quad \cdot \\ \cdot \quad\quad \cdot \quad\quad \cdot \\ a_{N1} \cdots a_{N2} \cdots a_{NM} \end{bmatrix} \begin{Bmatrix} T_1 \\ T_2 \\ \cdot \\ \cdot \\ \cdot \\ T_M \end{Bmatrix}$$

The least squares error method finds $T_1 \ldots T_M$ which minimizes

$$\sum_{i=1}^{N^1} |r_i|^2.$$

The solution to the least squares problem is well known and

$$\begin{Bmatrix} T_1 \\ T_2 \\ . \\ . \\ . \\ T_m \end{Bmatrix} = - (A^*A)^{-1} A^* \begin{Bmatrix} e_1 \\ e_2 \\ . \\ . \\ . \\ e_n \end{Bmatrix} \qquad \text{B.2}$$

Equation B.2 is in terms of complex numbers. The above blancing criterion was programmed on HP-9845 which does not have complex operations, but which handles matrix operations as part of the extended Basic which it uses as a language.

To facilitate the programming, an isomorphism ϕ between complex numbers C and 2 x 2 matrices is used. Define

$$\phi: \begin{pmatrix}\text{complex} \\ \text{numbers}\end{pmatrix} \longrightarrow \begin{pmatrix}2 \text{ x } 2 \text{ matrices}\end{pmatrix}$$

by

$$\phi(x + iy) = \begin{pmatrix} x & -y \\ y & x \end{pmatrix} \qquad \text{B.3}$$

$$i = \sqrt{-1}$$

Using (4.5), the influence matrix becomes

$$\begin{bmatrix} a^x_{11} & -a^y_{11} & a^x_{12} & -a^y_{12} & \cdots & a^x_{1m} & -a^y_{1m} \\ a^y_{11} & a^x_{11} & a^y_{12} & a^x_{12} & & a^y_{1m} & a^x_{1m} \\ . & & . & & & . & \\ . & & . & & & . & \\ . & & . & & & . & \\ a^x_{n1} & -a^y_{n1} & a^x_{n2} & -a^y_{n2} & & a^x_{nm} & -a^y_{nm} \\ a^y_{n1} & a^x_{n1} & a^y_{n2} & a^x_{n2} & \cdots & a^y_{nm} & a^x_{nm} \end{bmatrix} \qquad \text{B.4}$$

where

$$a_{ij}^{x} = \mathrm{Re}(a_{ij}) \quad a_{ij}^{y} = \mathrm{Im}\,(a_{ij})$$

The balance weights become

$$T_1 = \begin{bmatrix} T_1^x & -T_1^y \\ T_1^y & T_1^x \\ . & . \\ . & . \\ . & . \\ T_m^x & -T_m^y \\ T_m^y & T_m^x \end{bmatrix}$$

where

$$T_i^x = \mathrm{Re}\,(Ti) \qquad T_i^y = \mathrm{Im}\,(Ti) \qquad \text{B.5}$$

2. Constrained Balancing Using a Linear Programming Algorithm

Next, the balancing problem is formulated so that constraints may be placed on the size of Ti. The method used is contained in Pilkey, Bailey, Smith

The starting point is equation B.1.

$$\begin{Bmatrix} r_1^x \\ r_1^y \\ . \\ . \\ . \\ r_n^x \\ r_n^y \end{Bmatrix} = \begin{bmatrix} e_1^x & a_{11}^x & -a_{11}^y & & a_{1m}^x & -a_{1m}^y \\ e_1^y & a_{11}^y & a_{11}^x & & a_{1m}^y & a_{1m}^x \\ . & & & . & & \\ . & + & & . & & \\ . & & & . & & \\ e_n^x & a_{n1}^x & -a_{n1}^y & & a_{nm}^x & -a_{nm}^y \\ e_n^y & a_{n1}^y & a_{n1}^x & & a_{nm}^y & a_{nm}^x \end{bmatrix} \begin{Bmatrix} T_1^x \\ T_1^y \\ . \\ . \\ . \\ T_m^x \\ T_m^y \end{Bmatrix} \qquad \text{B.1}$$

The algorithm used is a mini-max technique. Here the problem will be to minimize the maximum residual runout.

Take ϕ so that

$$\begin{aligned} \phi &\geq |r_i^x| \quad ; \quad i = 1,2,.....,N \\ \phi &\geq |r_i^y| \quad ; \quad i = 1,2,.....,N \end{aligned} \tag{B.6}$$

So ϕ is greater than or equal to the magnitude of any runout (actually the x and y components of any runout). Finding balance weights T_i which minimize ϕ will in effect minimize the maximum runout the rotor will see.

B.1 and

$$\begin{aligned} \phi &\geq r_i^x \quad ; \quad i = 1,2,.....,N \\ \phi &\geq -r_i^x \quad ; \quad i = 1,2,.....,N \\ \phi &\geq r_i^y \quad ; \quad i = 1,2,.....,N \\ \phi &\geq -r_i^y \quad ; \quad i = 1,2,.....,N \end{aligned} \tag{B.7}$$

Then

$$\begin{aligned} \phi \geq r_i^x &= e_i^x + \sum_{k=1}^{M} (a_{ik}^x T_k^x - a_{ik}^y T_k^y) \\ \phi \geq -r_i^x &= -e_i^x - \sum_{k=1}^{M} (a_{ik}^x T_k^x - a_{ik}^y T_k^y) \\ \phi \geq r_i^y &= e_i^y + \sum_{k=1}^{M} (a_{ik}^y T_k^x + a_{ik}^y T_k^y) \\ \phi \geq -r_i^y &= -e_i^y - \sum_{k=1}^{M} (a_{ik}^y T_k^x + a_{ik}^x T_k^y) \end{aligned} \tag{B.8}$$

In B.8 ϕ and T_k are unknown. Writing B.8 as a linear programming problem it is minimize ϕ subject to

In B.8 ϕ and T_k are unknown. Writing B.8 as a linear programming problem it is minimize ϕ subject to

$$
\begin{aligned}
-\phi + \sum_{k=1}^{M} (a_{ik}^x T_k^x - a_{ik}^y T_k^y) &\leq -e_i^x \\
-\phi - \sum_{k=1}^{M} (a_{ik}^x T_k^x - a_{ik}^y T_k^y) &\leq e_i^x \\
-\phi + \sum_{k=1}^{M} (a_{ik}^y T_k^x + a_{ik}^y T_k^y) &\leq -e_i^y \\
-\phi - \sum_{k=1}^{M} (a_{ik}^y T_k^x + a_{ik}^x T_k^y) &\leq e_i^y
\end{aligned}
$$

To this we can easily add constraints on the balance weights.

$$
\begin{aligned}
T_i^x &\leq T_{max} \\
-T_i^x &\leq T_{max} \\
T_i^y &\leq T_{max} \\
-T_i^y &\leq T_{max}
\end{aligned}
\qquad \text{B.10}
$$

Writing B9 in matrix notation minus the constraints

$$
\begin{bmatrix}
-1 & a_{11}^x & -a_{11}^y & & a_{1m}^x & -a_{1m}^y \\
-1 & a_{11}^x & a_{11}^y & \cdots & -a_{1m}^x & a_{1m}^y \\
-1 & a_{11}^y & a_{11}^x & & a_{1m}^y & a_{1m}^x \\
-1 & a_{11}^y & a_{11}^x & & -a_{1m}^y & -a_{1m}^x \\
 & & \vdots & & \vdots & \\
-1 & a_{n1}^x & -a_{n1}^y & & a_{nm}^x & -a_{nm}^y \\
-1 & -a_{n1}^x & a_{n1}^y & \cdots & -a_{nm}^x & a_{nm}^y \\
-1 & a_{n1}^y & a^x{}_{n1} & & a^y_{nm} & a_{nm}^x \\
-1 & -a_{n1}^x & -a_{n1}^y & & -a_{nm}^y & -a_{nm}^x
\end{bmatrix}
\begin{Bmatrix}
\phi \\ T_1^x \\ \cdot \\ \cdot \\ \cdot \\ T_m^x \\ T_m^x
\end{Bmatrix}
\leq
\begin{Bmatrix}
-e_1^x \\ e_1^x \\ -e_1^y \\ \cdot \\ \cdot \\ \\ -e_n^x \\ e_n^x \\ -e_n^y \\ e_n^y
\end{Bmatrix}
$$

Add to this equation B.10 to obtain an algorithm to balance a rotor which constrains the balance weights.